1   **Revision 1**

2   **Experimental hydration of natural volcanic clinopyroxene phenocrysts under**

3   **hydrothermal pressures (0.5 – 3 kbar)**

4

5   **Franz A. Weis***

6   *Swedish Museum of Natural History, Dept. of Geosciences, SE-114 18 Stockholm, Sweden;*

7   *(franz.weis@nrm.se)*

8   *Uppsala University, Dept. of Earth Sciences, Center of Experimental Mineralogy, Petrology*

9   *and Geochemistry (CEMPEG), SE-752 36 Uppsala, Sweden*

10   **Roland Stalder**

11   *Innsbruck University, Inst. for Mineralogy and Petrography, A-6020 Innsbruck, Austria*

12   **Henrik Skogby**

13   *Swedish Museum of Natural History, Dept. of Geosciences, SE-114 18 Stockholm, Sweden*

14

15   *corresponding author

16

17   **Abstract**

18   Water is a key parameter in mantle rheology, magma genesis, magma evolution, and resulting

19   eruption styles, because it controls the density, the viscosity, as well as the melting and

20   crystallization behavior of a melt. The water content in nominally anhydrous minerals

21   (NAMs) such as clinopyroxene has recently been used as a proxy for magmatic water

22   contents. NAMs, however, may dehydrate during magma degassing and eruption. We

performed rehydration experiments on potentially degassed clinopyroxene phenocrysts from various volcanic settings. The experiments were conducted in hydrogen gas at 1 atm or hydrothermal pressures ranging from 0.5 to 3 kbar to test the incorporation of water into natural clinopyroxene under water fugacities similar to those in a volcanic system. Our results show a dependence of the water content in the clinopyroxene crystals with pressure as the phenocrysts begin to dehydrate upon lower water fugacities in the experiments. Water loss or gain in a crystal occurs according to the relatively fast redox-reaction $OH^- + Fe^{2+} \leftrightarrow O^{2-} + Fe^{3+} + \frac{1}{2} H_2$ which was confirmed by Mössbauer spectroscopy. The kinetics of this redox-process are independent of pressure and thus water fugacity. Water contents in rehydrated clinopyroxene crystals can be related to magmatic water contents at various levels in a volcanic system. Our results thus show that the water content in erupted clinopyroxene phenocrysts cannot be taken for granted to be representative of magmatic water contents prior to magma degassing. The conducted experiments indicate the simultaneous dehydration of clinopyroxene along with magma ascent and degassing. Rehydration experiments under hydrothermal pressures, however, may be able to reconstruct clinopyroxene water contents at crystallization prior to dehydration.

Keywords: NAMs**,** clinopyroxene, hydrogen, hydrothermal pressure, magmatic water content

<u>**Word count:**</u>

Abstract: 269 words

Main manuscript: 7888 words

Acknowledgements: 115 words

Figure captions: 543 words

1. Introduction

46

47   Water in nominally anhydrous minerals (NAMs) such as clinopyroxene and olivine is

48   important for mantle rheology, storage of water in the mantle as well as for estimation of the

49   volatile content in erupted lavas (e.g., Wade et al. 2008; Hamada et al. 2011; Lloyd 2014,

50   Weis et al. 2015). Hydrogen in clinopyroxene is incorporated in structural defects such as

51   cation vacancies (e.g. Mg^{2+} vs. $2H^+$) and charge deficiencies (e.g. Si^{4+} vs. $Al^{3+} + H^+$) where it

52   is bonded to oxygen and, regarded as an oxide component, can be expressed as water

53   concentration. Various studies have shown that upon ascent from the mantle or during

54   volcanic eruptions NAMs can dehydrate by hydrogen diffusion out of the crystals.

55   Experiments have indicated that such dehydration mainly occurs according to the relatively

56   fast and reversible redox reaction

57    $$OH^- + Fe^{2+} \leftrightarrow O^{2-} + Fe^{3+} + \tfrac{1}{2}\,H_2 \qquad (1)$$
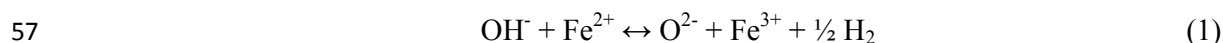
58   where the exchange of hydrogen ions (protons) is counterbalanced by a flux of electron holes

59   (e.g., Skogby and Rossman 1989; Skogby 1994; Bromiley et al. 2004; Koch-Müller et al.

60   2007; Sundvall and Skogby 2011). The kinetics of redox reaction (1) in pyroxenes in

61   particular have been well studied regarding hydration, dehydration and dependence on iron

62   content (Hercule and Ingrin 1999; Ingrin and Skogby 2000; Woods et al. 2000; Ingrin and

63   Blanchard 2006; Stalder and Skogby 2007; Sundvall et al. 2009; Sundvall and Skogby 2011).

64   Results from these studies demonstrate that hydrogen diffusion is strongly dependent on the

65   Fe-content and subsequent equilibration for clinopyroxenes with $X_{Fe/(Fe+Mg)} > 0.07$ occurs

66   within days to minutes at temperatures from 600 to 1000 °C, with kinetics similar to those of

67   hydrogen self-diffusion (H-D exchange; see reviews by Ingrin and Blanchard 2006 and Farver

68   2010). The hydrogen-associated defects in the crystal structure, however, will remain after the

69   redox-dehydration since reaction kinetics for vacancy and cation diffusion are many orders of

70   magnitude slower than the redox-processes (cf., Cherniak and Dimanov 2010). NAMs,

3   Weis et al. American Mineralogist

71 especially clinopyroxene phenocrysts in mantle xenoliths or volcanic rocks, are therefore

72 expected to keep a "memory" of their mantle hydrogen or the hydrogen content during

73 original crystallization from a magma. This difference in kinetics has also been exploited to

74 rehydrate natural and synthetic clinopyroxenes by performing rehydration experiments in

75 hydrogen gas at 1 atm and temperatures from 600 to 1000 °C (Skogby and Rossman 1989;

76 Sundvall et al. 2009; Sundvall and Skogby 2011; Weis et al. 2015). Testing the same approach

77 on fast erupted and partially dehydrated crystals from Tanganasoga volcano on El Hierro in

78 the Canary archipelago, however, gave the indication that a full rehydration of the crystals

79 was not possible at a pressure of only 1 atm. Water-rich clinopyroxenes from Tanganasoga

80 actually lose parts of their water content during annealing experiments in H_2 atmosphere.

81 Here we test the rehydration of Tanganasoga clinopyroxene crystals under pressures ranging

82 from 0.5 to 3 kbar, which would better represent conditions within the upper part of a volcanic

83 system. We further test this approach on a wider range of samples to study the rehydration

84 process in a more general sense. Additional samples include clinopyroxene from basanite and

85 ankaramite lavas from El Hierro and La Palma that were previously used for rehydration

86 experiments at 1 atm to estimate magmatic water contents (cf., Weis et al. 2015). In order to

87 get a comparison to clinopyroxene from Canary lava samples, clinopyroxene crystals of

88 different composition and from various other rock types and volcanic environments on Earth

89 and Mars are also included in the experiments.

90

91

92 ## 2. Samples

93 The majority of clinopyroxene crystals in this study come from the Canary Islands. More

94 precisely, rock samples included are El Hierro island ankaramite lava bombs from

95 Tanganasoga volcano and the Lomo Negro ankaramite lava flow (Carracedo et al 2001;

96   Longpre et al. 2009a; Villasante-Marcos and Pavón-Carrasco 2014). In addition, samples

97   from basanite lava flows and one kaersutite cumulate xenolith from the 1971 Teneguia

98   (Brändle et al. 1974) and 1949 Hoyo Negro (Klügel et al. 2000) eruptions on La Palma were

99   included. To get broad comparisons regarding geological environments and chemical

100   composition additional clinopyroxene from the 2006 andesite lava from Merapi volcano

101   (Gertisser 2001, Ratdomopurbo et al. 2013) on Java and basanite lavas from Shuangcai

102   volcano in Zejiang province, China (Liu et al., unpublished manuscript) were studied. Two

103   further samples consist of a mantle xenolith from Kilbourne Hole, New Mexico (Kil and

104   Wendlandt 2004; Harvey et al. 2012) and a specimen from the well-studied Martian Nakhla

105   meteorite (Bunch and Reid 1975; Treiman 1993). A full description of the samples used in this

106   study is given in Table 1.

107

108

109   **3. Methods**

110   Rock samples (n = 13) were crushed to obtain loose clinopyroxene crystals of a size

111   suitable for analysis (≥ 300 μm). These were hand-picked under a binocular microscope and

112   individual clinopyroxene crystals were then mounted in thermoplastic resin for further

113   processing. With the help of crystal morphology and optical microscopy (extinction angles),

114   the selected crystals (n = 37) were oriented along their crystallographic c-axis and their (100)

115   and (010) crystal faces, on which the directions of the main refractive indices (α, β and γ)

116   occur. A detailed procedure of the crystal alignment is described in Stalder & Ludwig (2007).

117   Various particle size-grades of Al_2O_3-grinding paper were used to thin and polish the oriented

118   crystals to a thickness of a few hundred micrometers.

119

120 **3.1. Electron probe micro analysis**

121   Analyses of major elements (Al, Ti, Fe, Mg, Na, K, Si, Ca, Mn, Cr) in

122 clinopyroxene crystals were carried out at the Department of Earth Sciences, Uppsala

123 University using a Field Emission-EPMA JXA-8530F JEOL hyperprobe. Between 5 and 8

124 spots were analyzed on each crystal using a beam current of 10 nA with an acceleration

125 voltage of 15 kV with 10 seconds on peak and 5 seconds on lower and upper background.

126 Standards used were fayalite (Fe_2SiO_4) for Fe, periclase (MgO) for Mg, pyrophanite

127 ($MnTiO_3$) for Mn and Ti, corundum (Al_2O_3) for Al, wollastonite ($CaSiO_3$) for Ca and Si,

128 eskolaite (Cr_2O_3) for Cr, nickel oxide (NiO) for Ni as well as albite ($NaAlSi_3O_8$), orthoclase

129 ($KAlSi_3O_8$) and apatite $Ca_5(PO_4)_3(OH,F,Cl)$ for Na, K and P, respectively. Several crystals

130 showed weak zonation in backscattered electron (BSE) images and for each crystal an average

131 composition was calculated from all analyzed spots. A detailed description of the EPMA

132 procedure and the analytical uncertainties is presented in Barker et al. (2015). From the

133 obtained weight percentages, the number of atoms per formula unit in each crystal was

134 calculated on the basis of a four cation-normalization. In order to distinguish between and

135 quantify Fe^{2+} and Fe^{3+} in clinopyroxenes, Mössbauer spectroscopy was applied (see section

136 3.4). Average compositional data for clinopyroxene from samples LP1971-1, LP1949 and

137 EH-Ank were taken from Weis et al. (2015).

138

139 **3.2. Rehydration experiments**

140 **3.2.1. Experimental strategy.** All rehydration experiments were performed at a temperature

141 of 700 °C, at which hydrogen diffusion coupled to redox reaction (1) has been shown to be

142 active (Skogby and Rossman 1989; Skogby 1994; Stalder and Skogby 2003; Bromiley et al.

143 2004; Koch-Müller et al. 2007; Sundvall et al. 2009; Sundvall and Skogby 2011).

144   Clinopyroxene crystals in this study show $X_{Fe/(Fe+Mg)} > 0.08$ (Table 2) and are thus above the

145   threshold value suggested by Hercule and Ingrin (1999) ($X_{Fe/(Fe+Mg)} > 0.07$). Therefore, the

146   hydration kinetics for equation (1) are expected to be similar to the kinetics for hydrogen self-

147   diffusion (Ingrin and Blanchard 2006). For rehydration it is also relevant how much Fe^{3+} is

148   present in the crystals. Fe^{3+} generated by the redox-process discussed above would probably

149   follow similar kinetics. Additional Fe^{3+} may have been incorporated during crystallisation by

150   other charge balancing mechanisms such as an aegirine component ($NaFe^{3+}$). This Fe^{3+},

151   however, seems to be more stable and to take part in the redox-processes only in association

152   with the occurrence of trivalent cations (e.g. Al^{3+}, Fe^{3+}) in the tetrahedral site, which are

153   associated with hydrogen defects (Skogby and Rossman 1989; Skogby 1994; Purwin et al.

154   2009). However, a component involving ($NaHFe^{2+}$) otherwise seems less likely. At 700 °C

155   the reaction kinetics for hydrogen self-diffusion are as high as $-logD = 11.3$ m^2/s and hence at

156   least 4.5 orders of magnitude higher than for vacancy diffusion ($-logD \leq 16$ m^2/s) (Hercule

157   and Ingrin 1999; Ingrin and Skogby 2000; Ingrin and Blanchard 2006; Cherniak and Dimanov

158   2010). Therefore, for the given temperature and time intervals, a relatively fast hydrogen

159   diffusion is expected, whereas defects other than those generated by the redox-process are not

160   expected to be significantly annealed. This is different to previous high-pressure and high-

161   temperature experiments where the hydrogen solubility in clinopyroxene has been tested (e.g.

162   Bromiley et al. 2004), where all structural defects are annealed. It is important to note that the

163   experimental conditions did not intend to mimic conditions in a natural magmatic system, but

164   simply to reverse redox reaction (1).

165   The rehydration experiments were not buffered in order to control the oxygen fugacity.

166   However, due to the hedenbergite component in the clinopyroxene crystals (see Table 2) we

167   assume that the oxygen fugacity is controlled by the hedenbergite-magnetite-quartz buffer,

168   which imposes redox conditions similar to QFM (cf. Gustafson 1974, Xirouchakis and

7   Weis et al. American Mineralogist

169   Lindsley 1998). Water fugacities for pressure experiments behave in a linear relation to and

170   do not deviate strongly from the nominal pressure (cf. Pitzer and Sterner 1994).

171

172   **3.2.2. Rehydration at 1 atm.** In order to rehydrate the defects in clinopyroxene that lost

173   hydrogen during oxidation (see Eq.1), the crystals were heated under a stream of H_2 gas for

174   different time intervals (see Table 3 for details) at a temperature of 700 °C and an ambient

175   pressure of 1 atm. The crystals were kept in a gold sample holder and placed into the middle

176   of a horizontal glass-tube furnace after the target temperature had been reached. The

177   temperature was measured with a Pt_{100}–$Pt_{90}Rh_{10}$ thermocouple placed directly above the

178   samples, which has an estimated uncertainty of ± 2 °C. Prior to the start of the hydrogen flow,

179   the glass tube was flushed with CO_2 so that reaction between the minerals and ambient

180   oxygen as well as an explosion-risk of the hydrogen gas was prevented. Clinopyroxenes were

181   then heated. After thermal annealing, the glass tube was again flushed with CO_2 and the

182   crystals were removed from the furnace. Heating and cooling times of the samples for this

183   method are on the order of ~1 minute.

184

185   **3.2.3. Rehydration under pressure.** For pressure experiments (Table 3), selected crystals

186   were welded into Au-capsules with an outer (inner) diameter of 5.0 (4.6) mm together with 12

187   μL of water. To prevent any dissolution of the clinopyroxene during the experiments, about 2

188   mg of diopside powder ($CaMgSi_2O_6$) were added to the capsule. Au-capsules were sealed

189   using a Lampert PUK U3 welding device (equipped with tungsten electrode, flushed with

190   argon gas). Possible leaks causing water loss were identified by weighing the capsules before

191   and after heating in an oven at 120 °C for 15 min. Pressure treatment was performed in Rene

192   41 steel-bombs in cold seal pressure vessels at Innsbruck University using water as pressure

193   medium. All experiments were performed at a temperature of 700 °C and pressures between

194   0.5 and 3 kbar (Table 3). The temperature was measured by Ni-CrNi thermocouples and

195   pressures were measured with a Heise gauge and kept constant within 0.05 kbar during the

196   whole run duration.

197

198   **3.3. FTIR spectroscopy**

199   Before and after thermal and/or hydrothermal treatment, polarized FTIR spectra

200   in the range 2000-5000 cm^{-1} were acquired on the oriented clinopyroxene crystals along the

201   directions of the main refractive indices (α, β and γ) to obtain the total absorbance:

202    $A_\alpha + A_\beta + A_\gamma = A_{total}$. A_α and A_γ were measured on the (010) crystal face and A_β on (100). The

203   polished crystals were measured in the sample compartment of a Bruker Vertex 70

204   spectrometer equipped with a NIR source (halogen lamp), a CaF_2 beamsplitter, a wiregrid

205   polarizer (KRS-5) and an InSb detector. Another set of crystals was measured at Innsbruck

206   University using a Bruker Hyperion 3000 microscope equipped with a Globar source, a KBr

207   beamsplitter and a MCT detector. Crystal thickness varied between 150 and 800 μm, with

208   most crystals having a thickness between 200 and 400 μm for both the (100) and (010)

209   orientations. Cracks and inclusions in the crystals were avoided by applying small apertures

210   (100 to 400 μm) for masking during analysis. In some cases impurities (e.g., magnetite

211   inclusions) were present in the beam path, but these appeared not to have had any significant

212   effect on the OH range of the spectra. For each individual spectrum, 128 scans were

213   performed and averaged. No significant differences between the analyses in the sample

214   compartment and microscope measurements were observed. The obtained spectra were

215   baseline corrected by a polynomial function and the individual OH bands were fitted with the

216   software PeakFit and used for further calculations. The corresponding water contents were

217   then calculated using both the wavenumber-dependent calibration function established by

218   Libowitzky and Rossman (1997) and the mineral-specific (augite) calibration of Bell et al.

219   (1995).

220

221   **3.4. Mössbauer spectroscopy**

222   The oxidation states of iron in clinopyroxenes before and, where possible, after the

223   rehydration experiments were obtained by Mössbauer spectroscopy. To obtain a sample

224   average for different iron valence states, powdered crystal separates were analyzed with a

225   ^{57}Co standard source (active diameter 5.0 mm), while selected single crystals were analyzed

226   using a point source (active diameter 0.5 mm) in order to investigate oxidation and reduction

227   during rehydration experiments. Several powdered crystals (10 mg in total) from individual

228   rock samples were mixed and ground with acrylic resin and pressed to a thin disc under mild

229   heat (150 °C) for analysis with the standard source. Untreated, oriented single crystals for the

230   point source were cut in half and one piece was used for rehydration experiments first. After

231   the annealing and FTIR analysis the individual single crystal pieces were powdered, mixed

232   and ground with thermoplastic resin and formed into a ~1 mm^3 cylinder that was mounted on

233   a strip of tape for analysis with the point source. The Mössbauer measurements were

234   performed at incident angles of 90° and 54.7° to the γ-rays for the point and the standard

235   source, respectively. All obtained spectra were calibrated against an α-Fe foil, folded and

236   reduced from 1024 to 512 channels. The spectra fitting was done with the Mössbauer spectral

237   analysis software MossA (cf., Prescher et al. 2012). During the fitting process, one doublet

238   each was assigned to Fe^{2+} and Fe^{3+} in the octahedral positions. From the area of the doublets,

239   the percentage of each oxidation state relative to the total iron content of the sample was

240   obtained, assuming similar recoil-free fractions for Fe^{2+} and Fe^{3+}. The estimated analytical

241   error for the obtained Fe^{m+}/Fe_{tot} ratios is ± 1 %. No crystal specific compositional analysis

242   was carried out on the Mössbauer sample set due to the destructive nature of sample

243 preparation. Mössbauer results for La Palma and El Hierro lava samples were taken from

244 Weis et al. (2015). Data for the Nakhla meteorite were taken from Dyar (2003) due to the

245 limited amount of sample material available.

246

247

248 **4. Results**

249 **4.1. Electron probe micro analysis**

250 The clinopyroxene chemical data obtained by EPMA are shown in Table 2. The

251 chemical composition of Tanganasoga clinopyroxenes was measured on a sample set separate

252 to the one taken for rehydration experiments and is represented as average values. The full

253 data set is available in Appendix A1. The analyzed clinopyroxenes from the Canary Islands (n

254 = 22) are all titanium-rich diopsides (2.5 to 3.3 wt. % TiO_2) (Table 2, Fig. 1) with Mg#

255 between 74 and 79 (mean = 78). With only very few exceptions, the individual crystals are

256 homogeneous in composition and show limited zonation. Differences in chemical

257 composition between crystals of individual rock samples occur on occasion. Clinopyroxenes

258 from Merapi, Shuangcai and Kilbourne Hole (n = 8) are also diopsides with Mg# from 76 to

259 82. The crystal from the Nakhla meteorite is an augite (Mg# = 62). The structural formulas for

260 clinopyroxene phenocrysts from this study are reported in Table 2.

261

262 **4.2. FTIR before rehydration**

263 All analyzed clinopyroxenes showed absorption maxima at 3630, 3530, and 3460 cm^{-1}

264 in the IR spectra (Fig. 2), which corresponds to the typical vibrational bands expected for OH

265 in diopside (e.g., Skogby 2006). The OH band at around 3630 cm^{-1} is prominent for E   α

11   Weis et al. American Mineralogist

266 and E   β, while the two bands around 3530 and 3460 cm^{-1} dominate for E   γ. This

267 infrared-pleochroic behavior is typical for clinopyroxene OH bands (Fig. 2) (e.g., Beran 1976)

268 and thus excludes the influence of possible OH-bearing impurities (e.g. hydrous minerals,

269 melt/fluid inclusions).

270   Infrared analyses before rehydration experiments revealed a significant spread in the

271 water content of the crystals from different rock samples (Table 3, Fig. 3). In some cases,

272 water contents of clinopyroxene within individual rock samples varied significantly despite

273 homogenous crystal chemistry. Water contents (given in ppm weight H_2O) for clinopyroxene

274 from Tanganasoga samples ranged from 141 ppm to 790 ppm. Clinopyroxenes from the Lomo

275 Negro and La Palma lava flows showed values between 36 and 364 ppm. Crystals from

276 Merapi volcano were completely dry with water contents below detection limit, while those

277 from Shuangcai volcano varied between 84 and 292 ppm. The crystals from mantle xenoliths

278 from Kilbourne Hole showed values from 357 to 379 ppm. The Martian clinopyroxene from

279 the Nakhla meteorite was also completely dry with a water content below detection limit.

280 Water contents corresponding to the spectra differed for the calibrations of Bell et al. (1995)

281 and Libowitzky and Rossman (1997). Values determined with the mineral-specific calibration

282 by Bell et al. (1995) were about 25 % higher, but the authors note that their mineral-specific

283 (augite) calibration is primarily valid for samples with similar OH-spectra. Our diopside

284 spectra are mostly do not show a strong band at ~3460 cm^{-1} for E   α and E   β and thus

285 differ from the spectra presented in Bell et al. (1995). We therefore used the values derived

286 through the calibration by Libowitzky and Rossman (1997), which has previously been used

287 successfully for synthetic as well as natural clinopyroxene samples (e.g., Stalder 2004; Stalder

288 and Ludwig 2007; Sundvall and Stalder 2011) and which was reconfirmed by Mosenfelder

289 and Rossman (2013).

290   Potential uncertainties for calculated water contents can arise from baseline correction

291   and and measurements of the crystal thickness. However, due to the quality of the spectra and

292   the relatively large thickness of the crystals a maximum error of ±10 % is assumed for the

293   precision of the calculated clinopyroxene water contents. In addition, the uncertainty

294   regarding the accuracy of the values due to the calibration for absorption coefficients is

295   another ±10 % (cf. Libowitzky & Rossman, 1997) resulting in an overall uncertainty of ±20

296   % for the calculated clinopyroxene water contents. No hydrogen diffusion profiles were

297   observed in the clinopyroxene crystals.

298

299   **4.2.1. FTIR after rehydration at 1 atm.** The thermal treatment caused no fractures or other

300   visible effects on the crystals. The absorption bands increased significantly in height in all

301   three directions (α, β, and γ) after thermal annealing in some samples while they decreased in

302   others. The strongest increase as well as decrease in absorbance was notably always observed

303   for the band at 3630 cm cm^{-1}. No change in band positions was observed, however. Treatment

304   in H_2-atmosphere at 1 atm led to different hydration trends in clinopyroxene crystals from

305   Tanganasoga. Water-poor crystals from sample T4 increased their hydrogen content to values

306   between 226 and 307 ppm, whereas crystals with higher water contents from samples T1, T2,

307   T3 (569 to 790 ppm) showed a decrease to hydrogen contents between 394 and 565 ppm.

308   Clinopyroxene from Lomo Negro and the kaersutite cumulate xenolith from La Palma

309   reached water contents between 241 and 434 ppm. The dry Merapi crystals increased to

310   values between 151 and 177 ppm. Clinopyroxene from Shuangcai also showed a decrease as

311   well as an increase in water contents with values between 142 and 183 ppm. One annealed

312   crystal from Kilbourne Hole showed no significant change in water content. The Nakhla

313   clinopyroxene increased to a water content of 16 ppm. Results for rehydration at 1 atm are

314   presented in Table 3.

315 **4.2.2. FTIR after rehydration under pressure.** During the pressure experiments some

316 crystals fractured along the cleavage planes and surfaces had to be re-polished. However, no

317 entire crystal had to be discarded. Results for rehydration under pressure are presented in

318 Table 4. Hydrothermal pressure annealing resulted exclusively in an increase in absorbance

319 with the same pattern as for thermal annealing at 1 atm. All crystals seem to be close to

320 saturation after 100-150 hours of annealing, and no important changes within the analytical

321 error of the water content occur or are to be expected. After pressure treatment Tanganasoga

322 crystals reached water contents between 747 and 1129 ppm. Clinopyroxene from La Palma

323 and Lomo Negro lava flows increased to values between 668 and 1180 ppm. Pressure

324 annealed cpx crystals from Merapi range between 712 and 794 ppm. Crystals from Shuangcai

325 and Kilbourne Hole revealed water contents between 425 and 704 ppm. The clinopyroxene

326 from Nakhla showed a water content of 134 ppm after pressure annealing.

327

328 **4.2.3. Hydrogen treatment of pressure annealed samples.** Several pressure annealed

329 clinopyroxene crystals from Tanganasoga (T3(3) and T4(5)), Lomo Negro (LN-3) and

330 Kilbourne Hole (KBH-cpx2) were again annealed at 1 atm and then showed a decrease in

331 water content between 20 and 56 %.

332

333 **4.3. Mössbauer spectroscopy**

334 The results for the Mössbauer spectroscopy of clinopyroxenes are shown in Tables 5

335 and 6. A representative spectrum with doublets for Fe^{2+} and Fe^{3+} is shown in Figure 4a. On

336 average, the analyzed clinopyroxenes in this study show Fe^{3+}/Fe_{tot} ratios between 18 and 39

337 %. Both, reduction and oxidation of iron is observed upon hydrogen treatment (Table 6).

338 Crystals that lost hydrogen during annealing showed an increase in Fe^{3+}/Fe_{tot} while those that

339   incorporated hydrogen showed a reduction of the same. Neither metallic iron, which would

340   indicate excessive reduction, nor oxidation products such as magnetite or hematite were

341   observed after the experiments.

342

343

344   **5. Discussion**

345   **5. Redox processes**

346   The variation in clinopyroxene water contents between individual rock samples, especially

347   from the same location, correlates with the Mössbauer results. For example, clinopyroxene

348   crystals in sample T4 from Tanganasoga show low water and higher Fe^{3+} contents than

349   crystals from Tangansoga sample T1 where crystals have much higher water and lower Fe^{3+}

350   contents. Mössbauer spectroscopy also shows that redox-reaction (1) was active during

351   annealing experiments and Mössbauer data for the studied Tanganasoga crystals demonstrate

352   reduction as well as oxidation of Fe^{3+} and Fe^{2+} after thermal annealing (Table 6). The increase

353   and decrease of Fe^{3+} parallels the change in water content in the crystals (Fig.5). Crystals that

354   incorporated hydrogen under thermal annealing at 1 atm in hydrogen gas or under pressure

355   annealing showed a reduction of Fe^{3+} and a decrease in Fe^{3+}/Fe_{tot}. The measured changes in

356   Fe^{3+}/Fe_{tot} for the two investigated crystals from sample T4 match, within error, the expected

357   changes in Fe^{3+}/Fe_{tot} based on the hydrogen incorporation during rehydration (Table 6). For

358   example, crystal T4(7) incorporated 908 ppm of water upon thermal annealing, which

359   corresponds to 0.022 atoms per formula unit (apfu). Considering the 1:1 ratio of redox-

360   reaction (1) this intake would imply a reduction of 0.022 apfu Fe^{3+} corresponding to a change

361   of 10.9 % in Fe^{3+}/Fe_{tot} (Fe_{tot} = 0.203 apfu). Mössbauer analysis revealed a change in Fe^{3+}/Fe_{tot}

362   of 9.2 % (corresponding to 0.019 apfu). Those clinopyroxene crystals that showed a loss of

15   Weis et al. American Mineralogist

363   hydrogen upon annealing at 1 atm revealed an increase in Fe^{3+}. The expected rise in Fe^{3+}/Fe_{tot},

364   matches again, within analytical error, the measured change in Fe^{3+}/Fe_{tot} obtained by

365   Mössbauer spectroscopy. The minor discrepancies in expected vs. measured changes could be

366   a consequence of small compositional differences between the investigated crystals and the

367   sample average determined by EMPA. However, the results confirm that the hydrogen

368   diffusion is linked to redox-reaction (1). Interesting is that hydrogen diffuses out of the

369   clinopyroxene at 1 atm and that the charge balancing oxidation of Fe^{2+} occurs despite the

370   strongly reducing hydrogen atmosphere in the glass tube furnace. This implies that the

371   hydrogen diffusion out of clinopyroxene crystals is not only influenced by their environment

372   (oxidizing vs. reducing) but is also pressure related.

373

5.1. De- and rehydration kinetics

375   **5.1.1. Dehydration kinetics.** Besides the obvious rehydration of crystals, a partial

376   dehydration is observed when untreated crystals with higher water contents from Tanganasoga

377   (> 550 ppm) and Shuangcai (> 220 ppm) or pressure-annealed crystals are treated in hydrogen

378   at 1 atm. The dehydration commences almost immediately upon annealing (Table 3), although

379   it seems to cease after about 40 hours of annealing leading to a stabilization of the water

380   content. Tanganasoga crystals dehydrate to values between 60 and 70 % of the crystals' pre-

381   annealing water content while Shuangcai crystals drop to values between 59 and 82 %. This

382   implies a dependence of the crystals' water contents on the prevailing water fugacity, and

383   further supports previous conclusions that NAMs equilibrate their water content with varying

384   fluid pressure (e.g., Hamada et al. 2011; Weis et al. 2015). Mössbauer data for Tanganasoga

385   crystals (Table 5) show that this partial dehydration occurs by the oxidation of Fe^{2+} according

386   to reaction (1). The oxidation takes place despite the reducing atmosphere provided by the

387   hydrogen. The kinetics for hydrogen diffusion in and out of clinopyroxene have been well

388   established (Ingrin et al. 1995; Hercule and Ingrin 1999; Woods et al. 2000; Sundvall and

389   Skogby 2011). The dehydration kinetics for clinopyroxene crystals annealed in hydrogen gas

390   were tested in detail with two crystals from Tanganasoga sample T3. The two crystals were

391   polished to a thickness of ~150 μm on the (010) crystal face and annealed at 700 °C for

392   various time intervals (Table 7). From the results diffusion coefficients as previously

393   described for one-dimensional diffusion through the two polished surfaces (cf., Carslaw and

394   Jäger 1959; Ingrin et al. 1995) were calculated using Fick's 2nd law

395
$$\frac{c_t}{c_0} = \frac{8}{\pi^2} \sum_{n=0}^{\infty} \left(\frac{1}{(2n+1)^2} e^{\left(\frac{-Dt(2n+1)^2 \pi^2}{4L^2} \right)} \right).$$

396   Calculated diffusion curves are shown in Fig.6. The rate of diffusion for the dehydration along

397   (010) is of the order –logD = 12.5 m^2/s. Clinopyroxenes from Tanganasoga have $X_{Fe/(Fe+Mg)}$ >

398   0.21 and thus at the given temperature of 700 °C the expected value for -logD along (010) is

399   12.6 ± 0.4 m^2/s (Hercule and Ingrin 1999; Woods et al. 2000). This shows that the pressure

400   related dehydration at 1 atm within hydrogen gas occurs at similar kinetics as the hydrogen

401   self-diffusion.

402

403   **5.1.2. Rehydration kinetics.** Similar as for the dehydration the results for the rehydration

404   experiments can be used to calculate the kinetics according to the equation

405
$$\frac{c_t}{c_0} = 1 - \frac{8}{\pi^2} \sum_{n=0}^{\infty} \left(\frac{1}{(2n+1)^2} e^{\left(\frac{-Dt(2n+1)^2 \pi^2}{4L^2} \right)} \right).$$

406   Since the kinetics for rehydration at 1 atm are already well described (e.g., Hercule and Ingrin

407   1999; Sundvall et al. 2009; Sundvall and Skogby 2011) focus will be put on the rehydration

408   under pressure. Plotting the diffusion curves for two crystals reveals values for –logD of 12.5

409   m^2/s and 13.1 m^2/s for (100) as well as 12.8 m^2/s for (010) (Fig. 6). The values obtained for

17   Weis et al. American Mineralogist

410   (010) are again similar to those for hydrogen self-diffusion at 700 °C and 1 atm considering

411   analytical error. However, hydrogen self-diffusion along (100) under these conditions is

412   supposed to occur at around $-logD = 11.3$ m^2/s (Hercule and Ingrin 1999) and thus about one

413   order of magnitude faster than calculated from our experimental data. Yet, the value of 12.5

414   m^2/s is close to the diffusion of hydrogen along (100) with $-logD = 13.1 \pm 0.4$ m^2/s determined

415   by Sundvall and Skogby (2011) during hydration experiments at 1 atm and 700 °C. Further,

416   Hercule and Ingrin (1999) report values between 12.8 and 13.7 m^2/s for hydrogen extraction-

417   incorporation processes in diopside, which is in good agreement with our obtained data.

418

419   **5.2. Rehydration at different pressures**

420   From the obtained data it is obvious that the rehydration under pressure results in higher water

421   contents in the crystals than for annealing at 1 atm. A positive relation between pressure and

422   clinopyroxene water content can be seen after the rehydration experiments (Fig. 7). The two

423   crystals that have been subsequently annealed at lower pressures (2 and 3 kbar then at 0.5

424   kbar and finally at 1 atm) showed water loss. Plotting the water contents obtained for

425   annealing experiments against the different pressures (1 atm to 3 kbar) on a logarithmic scale

426   reveals a positive correlation. A perfect relation between pressure and water content cannot be

427   seen for the total of the Tanganasoga crystals on first glance which might be due to minor

428   variations in crystal compositions (Table 3 and 4). However, plotting the average water

429   contents of annealed Tanganasoga clinopyroxene crystals for each pressure reveals a trend

430   similar to that observed for the individual crystals. The same pressure relation is observed for

431   clinopyroxene crystals from Shuangcai (sample SC-2). Samples from Lomo Negro and

432   Merapi annealed at different pressures do not show this trend very clearly. For Lomo Negro

433   crystals, which are very homogenous in composition, the trend still holds within the analytical

434   error. The three Merapi crystals annealed at pressure, on the contrary, show differences in

435   their compositions. Crystal MP-8 has significantly more tetrahedral Al^{3+} (Table 2) which is

436   most likely the reason for the high water content at 0.5 kbar compared to the other crystals at

437   2 kbar.

438

5.3. Reconstruction of initial water contents in clinopyroxenes

5.3.1 Rehydration limitations. The hypothesis behind the rehydration of clinopyroxenes

441   proposes that their "initial" water content, i.e. their equilibrium water content prior to possible

442   dehydration, can be restored. This has previously been tested in various studies with a variety

443   of different clinopyroxenes and annealing experiments conducted at 1 atm (Sundvall et al.

444   2009; Sundvall and Skogby 2011; Weis et al. 2015). It remains difficult to show to what

445   extent the initial water content of the crystals can be reached by performing rehydration

446   experiments. For example, de- and subsequent rehydration of synthetic iron-poor diopside

447   showed that only ~75 % of the crystal's initial water content could be restored (Sundvall et al.

448   2009). Despite this aspect of insufficient rehydration there might be also a risk of excessive

449   hydration of the clinopyroxene crystals. Synthetic, originally dry but Fe^{3+}-rich clinopyroxene

450   has been shown to incorporate substantial amounts of hydrogen upon annealing (Skogby

451   1994). Further, due to fast ascent with limited to no magma degassing and violent eruption at

452   Tanganasoga volcano (cf. Pinel and Jaupart 2000; Manconi et al. 2009; Stroncik et al. 2009;

453   Pedrazzi et al. 2014), the clinopyroxene crystals from the pyroclastic material most likely

454   were quenched. In this way, the crystals are expected to preserve their initial values (cf. Wade

455   et al. 2008). Yet, our rehydration experiments exceed the water contents in untreated crystals,

456   which might indicate an excessive hydration. Another issue is the possible effect which CO_2

457   and other volatiles might have on the water activity (e.g., Kovacs et al. 2012, Yang et al.

458   2014) and thus on the rehydration of hydrogen associated defects during the hydrothermal

459   experiments. However, there are also arguments against insufficient as well as excessive

460   rehydration.

461   The experiments, both de- and rehydration, conducted by Sundvall et al. (2009)

462   on very iron-poor crystals were performed at much higher temperatures (1000 °C) on a

463   timescale of several days. Due to much faster kinetics under these temperatures, vacancy and

464   cation diffusion is much more likely and cannot be excluded. The hydrogen incorporation was

465   not according to the 1:1 relation of redox-reaction (1) and despite that more hydrogen was

466   incorporated than Fe^{3+} was reduced, yet the original water content was not reached (Sundvall

467   et al. 2009). Considering that the 1:1 relation thus was not followed during dehydration either,

468   vacancy diffusion seems reasonable since the crystal otherwise would have been left without

469   a charge balance upon complete dehydration. The vacancy diffusion also could explain

470   hydrogen intake exceeding the Fe^{3+} reduction during rehydration. New defects such as

471   vacancies incorporating hydrogen were generated, however, not so many that the initial water

472   contents could be restored. Our crystals, on the contrary, are iron-rich. Any dehydration could

473   have easily been compensated by the oxidation of Fe^{2+}. Redox-processes in our experiment

474   also follow more closely the 1:1 relation of reaction (1) (Fig.5). In addition, experimental

475   conditions in this study make cation and vacancy diffusion very unlikely.

476   The risk of an excessive rehydration may mostly be linked to the amount of Fe^{3+}

477   available in the clinopyroxenes. The problem could be that additional available Fe^{3+}, which

478   has not been linked to prior dehydration, is reduced and hydrogen incorporated. The hydration

479   of initially dry, synthetic crystals by Skogby (1994) can be linked to the quantity of trivalent

480   cations in the tetrahedral site. The hydrogen intake of the crystals equals almost 1:1 the

481   amount of the latter (Skogby 1994). Mössbauer analysis further showed additional reduction

482   of Fe^{3+}, however, no additional hydrogen intake occurred. Also, as pointed out previously, not

483   all Fe^{3+} in the clinopyroxene crystals can be reduced since some of it may be for example

20   Weis et al. American Mineralogist

484   associated with an aegerine component, which only favors a $NaHFe^{2+}$ component in

485   association with defects suitable for hydrogen incorporation (cf. Skogby 1989, Purwin et al.

486   2009). Thus the defects become the limiting factor for the rehydration. Further, the synthetic

487   crystals in Skogby (1994) were grown under dry conditions which, however, are very unlikely

488   in a magmatic system.

489   The higher water contents in annealed Tanganasoga clinopyroxene compared to

490   untreated crystals could be a consequence of minor degassing of Tanganasoga magmas and

491   subsequent re-equilibration of the crystals to the new fluid pressure (e.g., Hamada et al. 2011).

492   Our experiments show that pressure differences cause significant changes in clinopyroxene

493   hydrogen content within a few hours. In addition, moderate dehydration by oxidation when

494   exposed to the atmosphere prior to quenching of the clinopyroxenes during eruption can be

495   assumed. Hydrogen diffusion in clinopyroxene is fast enough to evolve diffusion profiles over

496   several mm within minutes at magmatic temperatures (cf. Woods et al. 2000, Lloyd 2014) and

497   thus an effect of dehydration even on rapidly erupted crystals cannot be ruled out.

498   Dehydration upon eruption may be indicated by the variation in clinopyroxene water contents

499   (e.g. sample T2, $\Delta H_2O_{cpx} > 120$ ppm) within individual rock samples despite homogenous

500   crystal chemistry. Further, pressure annealed crystals from Shuangcai volcano reach water

501   contents similar to the highest values reported in clinopyroxenes from Gaoping volcano in the

502   Zhejiang province, China (Liu et al. unpublished manuscript) that are interpreted to have

503   preserved more often their initial water content, in contrast to the samples from Shuangcai

504   volcano where crystals are interpreted to have dehydrated.

505   Another issue regarding excessive hydration of the clinopyroxene crystals is the effect

506   of CO_2 on the activity of water. It has been shown that other volatiles such as CO_2 or halogens

507   within a magmatic system reduce the incorporation of hydrogen in NAMs (e.g., Stalder et al.

508   2008, Kovacs et al. 2012, Yang et al. 2014). As such, the water contents in olivines annealed

509 in a $H_2O + CO_2$ fluid phase, for example, were about half of those treated in pure H_2O (Yang

510 et al. 2014). However, these studies concentrated on the solubility of hydrogen in NAMs, and

511 the conducted experiments were done at pressures of several GPa and temperatures exceeding

512 1000 °C. Thus the annealed crystals experienced a resetting of their structural defects and the

513 influence of CO_2 on the generation of hydrogen associated defects was tested. Experimental

514 conditions in this study, however, do not intend a reset of hydrogen associated defects but

515 only a controlled reversal of redox-reaction (1) and thus a re-hydration of already existing yet

516 potentially dehydrated hydrogen associated defects.

517 Further, CO_2 activities in magmas from the Western Canaries might be low. Degassing

518 of mostly CO_2 dominated fluids (~90 %) commences at pressures above 1000 MPa in the

519 upper mantle while most clinopyroxene crystallization is below this level (500 to 800 MPa)

520 (e.g., Klügel et al. 2005, Longpré et al. 2008, Stroncik et al. 2009, Weis et al. 2015). Extensive

521 degassing of H_2O might only occur upon slow magma ascent in the shallower, i.e. crustal,

522 magma storage levels (e.g., Klügel et al. 2005, Longpré et al. 2008). A similar scenario may

523 be the case for the Merapi clinopyroxenes. The main zone of clinopyroxene crystallization

524 occurs between 300 and 600 MPa where most likely degassing of CO_2 and SO_2 from water-

525 rich magmas occurs (Costa et al. 2013, Chadwick et al. 2013). Exsolution and degassing of

526 water, on the contrary, has been modelled to commence below 300 MPa (Costa et al. 2013).

527 Thus the influence of CO_2 on the crystals in this study may initially have been low. A precise

528 effect of CO_2 or other volatiles on the rehydration experiments, however, is unknown and

529 remains to be tested.

530

531 **5.3.2 Corresponding magmatic water contents.** It has been shown that the water content in

532 clinopyroxene phenocrysts can be used to calculate the magmatic water content of their parent

533 melt by applying appropriate crystal/melt partitioning data (Wade et al. 2008; O'Leary et al.

534 2010; Nazzareni et al. 2011; Okumura 2011; Xia et al. 2013; Weis et al. 2015; Liu et al. in

535   review). This approach can be applied to test the validity of water contents in our rehydrated

536   crystals. The presumption is that the magmatic water content determined through rehydrated

537   clinopyroxenes correlates with values that are either observed or expected for the volcanic

538   environment they crystallized in.

539   For example, in order to determine parental magmatic water contents Weis et al.

540   (2015) performed rehydration experiments in hydrogen gas at 1 atm on clinopyroxenes from

541   ankaramite and basanite lava flows from the Western Canaries. Applying the equation by

542   O'Leary et al. (2010) ($\ln D$ = -4.2(±0.2) + 6(±0.5)^{VI}[Al^{3+}]-1(±0.2)[Ca^{2+}]) and compositional

543   data for clinopyoxene crystal/melt partition coefficients were calculated. From the partition

544   coefficients and water contents of clinopyroxene after rehydration experiments Weis et al.

545   (2015) determined parental H_2O contents between 0.71 ± 0.07 and 1.49 ± 0.15 wt. %. These

546   values corresponded well with data obtained from melt inclusions, glass and bulk rock

547   analyses from the Canaries and elsewhere as well as a feldspar-liquid hygrometer (Weis et al

548   2015). Experiments from the current study, however, clearly show that clinopyroxenes from

549   the same La Palma and El Hierro samples can reach significantly higher water contents under

550   pressure annealing which will have an effect on the calculated magmatic water contents. We

551   use the same approach presented in Weis et al. (2015) to calculate parental magmatic water

552   contents of rehydrated clinopyroxenes from this study. Magmatic water contents for La Palma

553   melts range from 3.96 ± 0.80 to 4.32 ± 0.86 wt. % (Table 8). For ankaramite melts from El

554   Hierro values between 2.84 ± 0.56 and 3.88 ± 0.78 wt. % H_2O are derived. This is

555   complemented with magmatic water contents between 1.25 ±0.24 and 6.34 ± 1.26 wt. % H_2O

556   for basaltic andesite from Merapi.

557   The values for magmatic water contents for the La Palma melts are considerably

558   higher than those determined by Weis et al. (2015) (0.71 ± 0.07 to 1.49 ± 0.15 wt. % H_2O)

559   and are more similar to melts from El Hierro's Tanganasoga volcano (2.84 ± 0.56 to 3.88 ±

560   0.78 wt. % H_2O) (Table 6). This overlap is expected considering that both islands are part of

561   the Western Canaries and that Tanganasoga melts can be seen as the volatile-rich primitive

562   magma source in the upper mantle (e.g., Manconi et al. 2009). Magmatic water contents for

563   ankaramite magmas from Teno volcano on Tenerife, a volcanic system similar to

564   Tanganasoga, have been estimated to have been up to 3 wt. % (Longpré et al. 2009b; Fig. 8)

565   supporting the high values obtained through pressure annealed clinopyroxenes. In addition,

566   magmatic water contents for the western Canaries can be estimated using compositional data

567   of amphibole and the thermobarometric formulations by Ridolfi and Renzulli (2012) (Eq. 1a

568   and 4). Using compositional data for amphibole pheno- and xenocrysts in basanite and

569   phonolite lavas from La Palma and the kaersutite cumulate xenolith from this study (sample

570   LP1971-B) (Klügel et al. 2000; Barker et al. 2015) reveals magmatic water contents between

571   3.37 ± 0.78 and 4.48 ± 0.78 wt. % (Appendix A1) with an average of 3.76 ± 0.78 wt. % H_2O.

572   These values overlap with the range obtained through pressure annealed clinopyroxene from

573   the Western Canaries. Most amphibole crystals in the 1971 lavas on La Palma are xenocrysts,

574   however, amphibole in the Western Canaries crystallizes at the same depth as the

575   clinopyroxene (20-45 km) (Klügel et al. 2005; Longpré et al. 2009a; Barker et al. 2015; Weis

576   et al. 2015). Thus the xenocrysts provide a guideline for the H_2O content in the volcanic

577   system at this depth. Further, the values obtained from amphibole phenocrysts in

578   phonotephrites (3.47 ± 0.78 to 4.48 ± 0.78 wt. % H_2O) from the 1949 eruption on La Palma

579   (Klügel et al. 2000) provide a direct comparison for magmatic water contents at depth.

580   Amphibole from sample LB1971-B reveals magmatic water contents between 3.25 ± 0.78 and

581   4.17 ± 0.78 wt. % while pressure annealed clinpyroxene revealed 4.32 ± 0.86 wt. % H_2O. The

582   available melt inclusion and volcanic glass data for the Canaries and other ocean island

583   basalts correspond to entrapment pressures between 0.3 and 0.5 kbar (e.g., Dixon et al. 1997;

584   Wallace 1998) which are far below the crystallization pressures of Western Canary

585   clinopyroxene (cf., Klügel et al. 2005; Longpré et al. 2009a; Barker et al. 2015; Weis et al.

586   2015). Thus the melt inclusions and water contents in clinopyroxene annealed at 1 atm may

587   represent the water contents in the upper parts of the volcanic system after potential H_2O loss

588   from the magma while pressure-annealed clinopyroxenes most likely represent the

589   undegassed magmatic water content at crystallization in the upper mantle.

590   Similar to the results from the Canaries, are the results for Merapi volcano. Merapi

591   clinopyroxenes rehydrated at 1 atm reveal magmatic water contents of 1.25 ± 0.24 and $1.46 \pm$

592   0.30 wt. %. These values overlap with melt inclusion data reported in the literature (Gertisser

593   2001; Nadeau et al. 2013; Preece et al. 2014; Fig.8). Most melt inclusions from Merapi are

594   considered to have undergone H_2O loss (Gertisser 2001; Preece et al. 2014), to be re-

595   equilibrated (Preece et al. 2014) or to be of secondary origin (Nadeau et al. 2013). Entrapment

596   and re-equilibration of the melt inclusions occurred at depth between 0.6 and 9.7 km (Nadeau

597   et al. 2013; Preece et al. 2014). Pressure-annealed clinopyroxene phenocrysts, however, reveal

598   magmatic water contents around 6.0 ± 1.2 wt. % which overlap with magmatic H_2O contents

599   determined through amphibole in the lava samples (~6.0 ± 0.9 wt. % H_2O; Costa et al. 2013;

600   Nadeau et al. 2013). Crystallization of host clinopyroxene and amphibole occurred much

601   deeper in the volcanic system between 14 and 25 km (Gertisser 2001; Chadwick et al. 2013;

602   Costa et al. 2013; Nadeau et al. 2013; Preece et al. 2014). Further, the clinopyroxene based

603   magmatic water contents fall within the range of water contents for vapor saturated basaltic

604   andesite at depth between 14 and 25 km (6 to 10 wt. % H_2O) (Pineau et al. 1998). The

605   magmatic water content of 2.66 ± 0.54 wt. % determined by crystal MP-8, annealed at 0.5

606   kbar, lies within range of values determined by melt inclusions. Together with clinopyroxene

607   annealed at 1 atm this samplerepresents the magmatic water contents in the shallower part of

608   the volcanic system after various stages of magma degassing. Phenocrysts annealed at higher

609   pressure, on the contrary, are representative for magmatic water contents at the depth of their

610   crystallization and prior to degassing.

611   One problem with comparing the clinopyroxene data to magmatic water

612   contents derived by amphibole is the timing of crystallization. NAMs and in this case

613   clinopyroxene usually crystallize earlier than amphibole. Significant fractionation of NAMs

614   thus might enrich the residual melt in H_2O which then leads to the onset of amphibole

615   crystallization. Thus the comparison of the two minerals might actually indicate an excessive

616   rehydration of the crystals. However, especially for Merapi modelling showed that amphibole

617   and clinopyroxene crystallization occurred simultaneously (e.g., Costa et al. 2013). Most

618   Merapi clinopyroxenes in this study are low in Al_2O_3 (Table 2). The low-Al clinopyroxene has

619   been determined by thermobarometry and modelling to have crystallized in the main magma

620   storage level between 10 and 20 km depth (300 to 600 MPa) together with amphibole and

621   plagioclase at magmatic water contents between 4 and 6 wt.% (Chadwick et al. 2013, Costa et

622   al. 2013, Nadeau et al. 2013). Amphibole and high-Al clinopyroxene crystallization already

623   commences at deeper levels (Costa et al. 2013). Results from plagioclase-melt hygrometry

624   indicate magmatic water content of 5.0 ±0.5 wt. % in the main magma storage zone (Surono

625   et al. 2012). Thus the comparison of magmatic water contents derived through amphibole and

626   clinopyroxene seems applicable. However, it remains difficult to establish similar relations

627   between clinopyroxene and amphibole for the samples from the Canary Islands. The

628   phonotephrites of the 1949 eruption are seen as a separate magma batch compared to the

629   basanites (Klügel et al. 2000). Also crystals of both minerals in the kaersutite cumulate

630   sample LP1971-B were accumulated from the same magma but it is not known if they

631   actually crystallized simultaneously (Barker et al. 2015). Similar, feldspar hygrometry from

632   the La Palma basanites indicates a water content of around 4 wt. % in the magma, but

633   crystallization most likely occurred after clinopyroxene (Barker et al. 2015). However, the

634   three independent methods all point towards water contents between 3 and 4 wt. %. Further,

635   the highest water contents among untreated clinopyroxene crystals from Tanganasoga would

636   result in magmatic water contents close to 3 wt. % and again overlap with values derived

26   Weis et al. American Mineralogist

637   through rehydrated crystals. As outlined above, dehydration of the Tanganasoga crystals upon

638   magma degassing and eruption cannot be excluded, which would indicate even higher

639   magmatic water contents at depth.

640   It cannot be claimed with entire certainty that our rehydration experiments

641   reconstructed the actual initial water contents of clinopyroxenes prior to possible dehydration.

642   However, our results outlined above indicate that it is likely the case.

643

644

645   **6. Implications**

646   The rehydration experiments conducted in this study imply that clinopyroxene crystals begin

647   to dehydrate upon magma ascent within a volcanic system. This dehydration is a consequence

648   of the decrease in pressure with vicinity to the surface and the adaption of the crystals to the

649   new conditions. Further, the crystals may undergo dehydration through oxidation during the

650   eruption, and eventually may fully dehydrate. Both types of dehydration occur according to

651   redox-reaction (1). Thus the water content of erupted clinopyroxene phenocrysts cannot be

652   taken for granted as a proxy for magmatic or mantle water contents. The pressure and

653   oxidation related dehydration may be hindered by fast magma ascent with minimal magma

654   degassing and more violent eruptions which subsequently lead to quenching of the erupted

655   crystals. In this way the initial water content at crystallization may be preserved to large

656   extents. In order to reach a rehydration, corresponding to the water content at crystallization,

657   of dehydrated clinopyroxene phenocrysts, experiments at 1 atm in hydrogen gas are not

658   sufficient. It requires the input of pressure to restore water contents of clinopyroxene in the

659   mantle. A precise threshold value for pressure at which the water content in clinopyroxene

660   will be held stable has not been established. Further, investigation of rehydration at different

661 pressures in comparison with detailed studies on the crystals' origin and eruption history

662 could help to establish a more precise relation between pressure and clinopyroxene water

663 content. The rehydration at different pressures of dehydrated clinopyroxene phenocrysts from

664 lava samples seems to be able to serve as a proxy for magmatic water contents at different

665 levels in a volcanic system. Thus different pressure experiments could be used to investigate

666 the degassing history of magma in a volcanic system which, in turn, has implications on

667 petrological processes.

668

669

7. Acknowledgments

680   **References**

681   1. Barker, A.K., Troll, V.R., Carracedo, J.-C. and Nicholls, P.A. (2015) The magma

682   plumbing system for the 1971 Tenguía eruption, La Palma, Canary Islands.

683   Contributions to Mineralogy and Petrology, 170, 54, doi:10.1007/s00410-015-1207-7.

684   2. Bell, D. R., Ihinger, P.D. and Rossman, G.R. (1995) Quantitative analysis of trace OH

685   in garnet and pyroxenes. American Mineralogist, 80, 465-474.

686   3. Beran, A. (1976) Messung des Ultrarot-Pleochroismus von Mineralen. XIV. Der

687   Pleochroismus der OH-Streckfrequenz in Diopsid. Tschermaks Mineralogische und

688   Petrographische Mitteilungen, 23, 79-85.

689   4. Brändle, J. L., Fernandez Santin, S. and Lopez Ruiz, J., (1974) Mineralogy Of The

690   Materials From Teneguía Volcano, La Palma, Canary Islands. Estudios Geologicos

691   (Madrid,) Vol. Teneguía, 41-47.

692   5. Bromiley, G.D., Keppler, H., McCammon, C., Bromiley, F.A. and Jacobsen, S.D.

693   (2004) Hydrogen solubility and speciation in natural, gemquality chromian diopside.

694   American Mineralogist, 89, 941–949.

695   6. Bunch, T.E. and Reid, A.M. (1975) The nakhlites, part 1: Petrography and mineral

696   chemistry. Meteoritics, 10, 303-315.

697   7. Carracedo, J.C., Badiola, E.R., Guillou, H., de La Nuez, J. and Pérez Torrado, F.J.

698   (2001) Geology and volcanology of La Palma and El Hierro, Western Canaries.

699   Estudios Geologicos, 57, 175– 273.

700   8. Carslaw, H.S. and Jäger, J.C. (1959) Conduction of heat in solids. Clarendon Press,

701   Oxford, UK.

702   9. Chadwick, J.P., Troll, V.R., Waight, T.E., van der Zwan, F.M. and Schwarzkopf, L.M.

703   (2013) Petrology and geochemistry of igneous inclusions in recent Merapi deposits: a

704   window into the sub-volcanic plumbing system. Contributions to Mineralogy and

705   Petrology, 165, 259-282.

706   10. Cherniak, D.J. and Dimanov, A. (2010) Diffusion in pyroxene, mica and amphibole.

707   Reviews in Mineralogy and Geochemistry, 72, 641-690.

708   11. Costa, F., Supriyati, A., Bouvet de Maisonneuve, C. and Pallister, J.S. (2013)

709   Petrological insights into the storage conditions, and magmatic processes that yielded

710   the centennial 2010 Merapi explosive eruption. Journal of Volcanology and

711   Geothermal Research, 262, 209-235.

712   12. Dixon, J.E., Clague, D.A., Wallace, P. and Poreda, R. (1997) Volatiles in alcalic

713   basalts from the North Arch Volcanic Field, Hawaii: extensive degassing of deep

714   submarine-erupted alkali series lavas. Journal of Petrology, 38, 911-939.

715   13. Dyar, M.D. (2003) Ferric iron in SNC meteorites as determined by Mössbauer

716   spectroscopy: Implications for martian landers and martian oxygen fugacity.

717   Meteoritics and Planetary Science, 38, 1733–1752.

718   14. Farver, J.R. (2010) Oxygen and Hydrogen Diffusion in Minerals. Reviews in

719   Mineralogy and Geochemistry, 72, 447-507.

720   15. Gertisser, R. (2001) Gunung Merapi (Java, Indonesien): Eruptionsgeschichte und

721   magmatische Evolution eines Hochrisiko-Vulkans, 394 p. Ph.D. thesis Universität

722   Freiburg (in German).

723   16. Gustafson, W.I. (1974) The stability of andradite, hedenbergite, and related minerlas

724   in the system Ca-Fe-Si-O-H. Journal of Petrology, 15, 455-496.

725   17. Hamada, M., Kawamoto, T., Takahashi, E. and Fujii, T. (2011) Polybaric degassing of

726   island arc low-K tholeiitic basalt magma recorded by OH concentrations in Ca-rich

727   plagioclase. Earth and Planetary Science Letters, 308, 259-266.

728   18. Harvey, J., Yoshikawa, M., Hammond, S.J. and Burton, K.W. (2012) Deciphering the

729   trace element characteristics in Kilbourne Hole peridotite xenoliths: melt-rock

730   interaction and metasomatism beneath the Rio Grande Rift, SW USA. Journal of

731   Petrology, 53, 1709-1742.

732 19. Hercule, S. and Ingrin, J. (1999) Hydrogen in diopsides: Diffusion, kinetics of

733   extraction-incorporation, and solubility. American Mineralogist, 84, 1577-1587.

734 20. Ingrin, J., Hercule, S. and Charton, T. (1995) Diffusion of hydrogen in diopside:

735   Results of dehydration experiments, Journal of Geophysical Research, 100, 489-499.

736 21. Ingrin, J. and Skogby, H. (2000) Hydrogen in nominally anhydrous upper-mantle

737   minerlas: concentration levels and implications. European Journal of Mineralogy, 12,

738   543-570.

739 22. Ingrin, J. and Blanchard, M. (2006) Diffusion of hydrogen in minerals. Reviews in

740   Mineralogy and Geochemistry, 62, 291–320.

741 23. Kil, Y. and Wendlandt, R.F. (2004) Pressure and temperature evolution of upper

742   mantle under the Rio Grande rift. Contributions to Mineralogy and Petrology, 148,

743   2665-2680.

744 24. Klügel, A., Hoernle, K.A., Schmincke, H.-U. and White, J.D.L. (2000) The

745   chemically zoned 1949 eruption on La Palma (Canary Islands): Petrologic evolution

746   and magma supply dynamics of a rift zone eruption. Journal of Geophysical Research,

747   105, 5997-6016.

748 25. Klügel, A., Hansteen, T.H. and Galipp, K. (2005) Magma storage and underplating

749   beneath Cumbre Vieja volcano,La Palma (Canary Islands). Earth and Planetary

750   Science Letters, 236, 211– 226.

751 26. Koch-Müller, M., Abs-Wurmbach, I., Rhede, D., Kahlenberg, V. and Matsyuk, S.

752   (2007) Dehydration experiments on natural omphacites: qualitative and quantitative

753   characterization by various spectroscopic methods. Physics and Chemistry of

754   Minerals, 34, 663–678.

755   27. Kovács, I., Green, D.H., Rosenthal, A., Hermann, J., O'Neill, H.S.C., Hibberson,

756   W.O. and Udvardi, B. (2012) An experimental study of water in nominally anhydrous

757   minerals in the upper mantle near the water-saturated solidus. Journal of Petrology,

758   53, 2067–2093.

759   28. Libowitzky, E. and Rossman, G.R. (1997) An IR absorption calibration for water in

760   minerals. American Mineralogist, 82, 1111–1115.

761   29. Lloyd, A.S. (2014) Timescales of magma ascent during explosive eruptions: Insights

762   from the re-equilibration of magmatic volatiles, 176 p. Ph.D. thesis, Columbia

763   University, New York.

764   30. Longpré, M.A., Troll, V.R. and Hansteen, T.H. (2008) Upper mantle magma storage

765   and transport under a Canarian shield-volcano, Teno, Tenerife (Spain), Journal of

766   Geophysical Research, 113, B08203, doi:10.1029/2007JB005422.

767   31. Longpré, M.A., Troll, V.R., Hansteen, T.H. and Anderson, E. (2009a) Ankaramitic

768   Lavas and Clinopyroxene Megacrysts From the Tanganasoga Volcano, El Hierro

769   Island (Canary Archipelago). Eos Transactions AGU, 90(52), Fall Meet. Suppl.,

770   Abstract V51A-1662.

771   32. Longpré, M.A., Troll, V.R., Walter, T.R. and Hansteen, T.H. (2009b) Volcanic and

772   geochemical evolution of the Teno massif, Tenerife, Canary Islands: Some

773   repercussions on giant landslides on ocean island magmatism. Geochemistry

774   Geophysics Geosystems, 10, Q12017, doi:10.1029/2009GC002892.

775   33. Manconi, A., Longpré, M.A., Walter, T.R., Troll, V.R. and Hansteen, T.H. (2009) The

776   effects of flank collapses on volcano plumbing systems. Geology, 37, 1099-1102.

777   34. Morimoto, N., Fabries, J., Ferguson, A.K., Ginzburg, I.V., Ross, M., Seifert, F.A.,

778   Zussman, J., Aoki, K. and Gottardi, G. (1988) Nomenclature of pyroxenes. American

779   Mineralogist, 73, 1123-1133.

780   35. Mosenfelder, J. and Rossman, G.R. (2013) Analysis of hydrogen and fluorine in
781   pyroxenes: II. Clinopyroxene. American Mineralogist, 98, 1042-1054.

782   36. Nadeau, O., Williams-Jones, A.E. and Stix, J. (2013) Magmatic-hydrothermal
783   evolution and devolatilization beneath Merapi volcano, Indonesia. Journal of
784   Volcanology and Geothermal Research, 261, 50-68.

785   37. Nazzareni, S., Skogby, H. and Zanazzi, P. F. (2011) Hydrogen content in
786   clinopyroxene phenocrysts from Salina mafic lavas (Aeolian arc, Italy). Contributions
787   to Mineralogy and Petrology, 162, 275-288.

788   38. O'Leary, J.A., Gaetani, G.A. and Hauri, E.H. (2010) The effect of tetrahedral Al^{3+} on
789   the partitioning of water between clinopyroxene and silicate melt. Earth and Planetary
790   Science Letters, 297,111-120.

791   39. Okumura, S. (2011) The H_2O content of andesitic magmas from three volcanoes in
792   Japan, inferred from the infrared analysis of clinopyroxene. European Journal of
793   Mineralogy, 23, 771-778.

794   40. Pedrazzi, D., Becerril, L., Martí, J., Meletlidis, S., Galindo, I. (2014) Explosive felsic
795   volcanism on El Hierro (Canary Islands). Bulletin of Volcanology,76, 863.

796   41. Pineau, F., Shilobreeva, S., Kadik, A. and Javoy, M. (1998) Water solubility and D/H
797   fractionation in the system basaltic andesite-H_2O at 1250°C and between 0.5 and 3
798   kbars. Chemical Geology, 147, 173-184.

799   42. Pinel, V., and Jaupart, C., (2000) The effect of edifice load on magma ascent beneath
800   a volcano. Philosophical Transactions of the Royal Society A - Mathematical,
801   Physical and Engineering Sciences, 358, 1515–1532.

802   43. Pitzer, K.S., Sterner, S.M. (1994) Equation of state valid continuously from zero to
803   extrem pressures for H_2O and CO_2. Journal of Chemical Physics, 101,3111-3116.

804   44. Preece, K., Gertisser, R., Barclay, J., Berlo, K. and Herd, R.A. (2014) Pre- and syn-
805   eruptive degassing n crystallisation processes of the 2010 and 2006 eruptions of
806   Merapi volcano, Indonesia. Contributions to Mineralogy and Petrology, 168, 1061.

807   45. Prescher, C., McCammon, C. and Dubrovinsky, L. (2012) MossA: a program for
808   analyzing energy-domain Mössbauer spectra from conventional and synchrotron
809   sources. Journal of Applied Crystallography, 45, 329-331.

810   46. Purwin, H., Stalder, R., Skogby, H. (2009) Hydrogen incorporation in Fe- and Na-
811   doped diopsides. European Journal of Mineralogy, 21, 691-704.

812   47. Ratdomopurbo, A., Beauducel, F., Subandriyo, J., Made Agung Nandaka, I.G.,
813   Newhall, C.G., Sayudi, D.S., Suparwaka, H. (2013) Overview of the 2006 eruption of
814   Mt. Merapi. Journal of Volcanology and Geothermal Research, 261, 87-97.

815   48. Ridolfi, F. and Renzulli, A. (2012) Calcic amphiboles in calc-alkaline and alkaline
816   magmas: thermobarometric and chemometric empirical equations valid up to 1130 °C
817   and 2.2 GPa. Contributions to Mineralogy and Petrology, 163, 877–895.

818   49. Skogby, H. (1994) OH incorporation in synthetic clinopyroxenes. American
819   Mineralogist, 79, 240–249.

820   50. Skogby, H. (2006) Water in natural mantle minerals I: pyroxenes. Reviews in
821   Mineralogy and Geochemistry, 62, 155–168.

822   51. Skogby, H. and Rossman, G.R. (1989) OH- in pyroxene: an experimental study of
823   incorporation mechanisms and stability. American Mineralogist, 74, 1059–1069.

824   52. Stalder, R. and Skogby, H. (2003) Hydrogen diffusion in natural and synthetic
825   orthopyroxene. Physics and Chemistry of Minerals, 30, 12-19.

826   53. Stalder, R. and Skogby, H. (2007) Dehydration mechanisms in synthetic Fe-bearing
827   enstatite. European Journal of Mineralogy, 19, 201-216.

828   54. Stalder, R. (2004) Influence of Fe, Cr and Al on hydrogen incorporation in
829   orthopyroxene. European Journal of Mineralogy, 16, 703–711.

830   55. Stalder, R. and Ludwig, T. (2007) OH incorporation in synthetic diopside. European

831   Journal of Mineralogy, 19, 373-380.

832   56. Stalder, R., Kronz, A. and Simon, K. (2008) Hydrogen incorporation in enstatite in the

833   system $MgO-SiO_2-H_2O-NaCl$. Contributions to Mineralogy and Petrology, 156, 653-

834   659.

835   57. Stroncik, N.A., Klügel, A. and Hansteen, T.H. (2009) The magmatic plumbing system

836   beneath El Hierro (Canary Islands): constraints from phenocrysts and naturally

837   quenched basaltic glasses in submarine rocks. Contributions to Mineralogy and

838   Petrology, 157, 593–607.

839   58. Sundvall, R. and Stalder, R. (2011) Water in upper mantle pyroxene megacrysts and

840   xenocrysts: A survey study. American Mineralogist, 96, 1215 - 1227.

841   59. Sundvall R., Skogby, H. and Stalder, R. (2009) Dehydration-hydration mechanisms in

842   synthetic Fe-poor diopside. European Journal of Mineralogy, 21, 17-26.

843   60. Sundvall, R. and Skogby, H. (2011) Hydrogen defect saturation in natural pyroxene.

844   Physics and Chemistry of Minerals, 38, 335–344.

845   61. Surono, J.P., Pallister, J., Boichu, M., Buongiorno, M.F., Budisantoso, A., Costa, F.,

846   Andreastuti, S., Prata, F., Schneider, D., Clarisse, L., Humaida, H., Sumarti, S.,

847   Bignami, C., Griswold, J., Carn, S. and Oppenheimer, C. (2012) The 2010 explosive

848   eruption of Java's Merapi volcano - a '100-year' event. Journal of Volcanology and

849   Geothermal Research 241-242, 121-135.

850   62. Treiman, A.H. (1993) The parent magma of the Nakhla (SNC) meteorite, inferred

851   from magmatic inclusions. Geochimica et Cosmochimica Acta, 57, 4753-4767.

852   63. Villasante-Marcos, V. and Pavón-Carrasco, F.J. (2014) Palaeomagnetic constraints on

853   the age of Lomo Negro volcanic eruption (El Hierro, Canary Islands). Geophysical

854   Journal International, 199, 1497-1514.

855   64. Wade, J.A., Plank, T., Hauri, E.H., Kelley, K.A., Roggensack, K. and Zimmer, M.
856   (2008) Prediction of magmatic water contents via measurement of H_2O in
857   clinopyroxene phenocrysts. Geology, 36, 799-802.

858   65. Wallace, P.J. (1998) Pre-eruptive H_2O and CO_2 contents of mafic magmas from the
859   submarine to emergent shield stages of Gran Canaria. In: P. P. E. Weaver, H.-U.
860   Schmincke, J. V. Firth and W. Duffield (eds.): Proceedings of the Ocean Drilling
861   Program, Scientific Results, 157, 411-420.

862   66. Weis, F.A., Skogby, H., Troll, V.R., Deegan, F.M. and Darehn, B. (2015) Magmatic
863   water contents determined through clinopyroxene: Examples from the Western Canary
864   Islands, Spain. Geochemistry Geophysics Geosystems, 16, 2127–2146.

865   67. Woods, S.C., Mackwell, S. and Dyar, D. (2000) Hydrogen in diopside: diffusion
866   profiles, American Mineralogist, 85, 480-487.

867   68. Xia, Q.K., Liu, J., Liu, S., Kovacs, I., Feng, M. and Dang, L. (2013) High water
868   content in Mesozoic primitive basalts of the North China Craton and implications on
869   the destruction of cratonic mantle lithosphere. Earth and Planetary Science Letters, 36,
870   85-97.

871   69. Xirouchakis, D., Lindsley, D.H. (1998) Equilibria among titanite, hedenbergite,
872   fayalite, quartz, ilmenite, and magnetite: Experiments and internally consistent
873   thermodynamic data for titanite. American Mineralogist, 83, 712-725.

874   70. Yang, X., Liu, D. and Xia, Q. (2014) CO2-induced small water solubility in olivine
875   and implications for properties of the shallow mantle. Earth and Planetary Science
876   Letters, 403, 37-47.

877   **Figure captions**

878   Figure 1: Compositional classification of clinopyroxenes shows most crystals from this study

879   to plot in or close to the diopside field. Only Nakhla clinopyroxene has an augite composition

880   (diagram after Morimoto et al. 1988).

881

882   Figure 2: Representative IR-spectra of clinopyroxene before (dashed line) and after (solid

883   line) annealing at pressure. Polarized measurements with E α and E γ were done on the

884   (010) crystal face while E β was measured on (100). Absorbances have been normalized to

885   1 mm thickness. The spectra show the three main vibrational bands of water at 3630 cm^{-1},

886   3530 cm^{-1}, 3460 cm^{-1}, which are expected for diopside (Skogby 2006) and relate to different

887   OH-dipole orientations (see text for details). The increase in peak intensity and thus water

888   content after pressure annealing is apparent.

889

890   Figure 3: Distribution of measured water contents for clinopyroxene crystals from this study

891   before and after thermal annealing at 1 atm and under pressure. Some crystals lose water upon

892   treatment in hydrogen gas at 1 atm. Water contents increase drastically in all samples upon

893   pressure annealing. Error bars represent the 20 % error from the FTIR analysis.

894

895   Figure 4: Representative Mössbauer spectra for clinopyroxene in sample T4(7) from

896   Tanganasoga volcano. a) Mössbauer spectrum of the sample before pressure annealing at 2

897   kbar and 700 °C. The spectrum shows the typical Fe^{2+} and Fe^{3+} doublets which were used to

898   determine the concentration of both iron oxidation states in the crystal. b) Comparison

899   between the fitted lines before and after 100 hours of pressure annealing. A decrease in Fe^{3+}

900   after the annealing can be observed.

37   Weis et al. American Mineralogist

901   Figure 5: Correlation between hydrogen loss or gain and redox processes within

902   clinopyroxene during annealing experiments. The change in Fe^{3+} and the loss or gain of

903   hydrogen atoms in the clinopyroxenes follows almost perfectly the 1:1 relation proposed by

904   redox-reaction (1) (see text for details).

905

906   Figure 6: Diffusion curves for dehydration of clinopyroxene in hydrogen gas at 1 atm (a and

907   b) and rehydration at different pressures (c, d, e and f) at 700 °C. For e) the value for c_{sat} was

908   taken as the average of the two highest concentrations in the crystal. Error bars represent the

909   10 % error for the precision of the FTIR analysis. All values for –logD (D as m^2/s) fall within

910   a narrow range and are similar to those obtained in previous studies (see text for details).

911

912   Figure 7: Relation between pressure and clinopyroxene water content. With increasing

913   pressure the water content in clinopyroxene crystals increases according to a logarithmic

914   trend. Solid lines represent trends for crystal populations in individual rock samples. Dashed

915   lines represent trends for individual crystals. Error bars represent the 20 % error of the FTIR

916   analysis.

917

918   Figure 8: Distribution of calculated water contents for parental melts for clinopyroxene from

919   a) El Hierro and La Palma b) Merapi volcano. Magma H_2O contents calculated on the basis of

920   pressure annealed clinopyroxenes from the western Canaries and Merapi correlate well with

921   magmatic water contents at greater depth for these volcanic systems derived through

922   amphiboles. Clinopyroxenes annealed at 1 atm in hydrogen, on the contrary, overlap more

923   with melt inclusion data which represents more the upper part of these volcanic systems. The

924   color gradient in the box indicates the frequency of magmatic water contents derived through

925   Merapi melt inclusions.

926   **Figures**
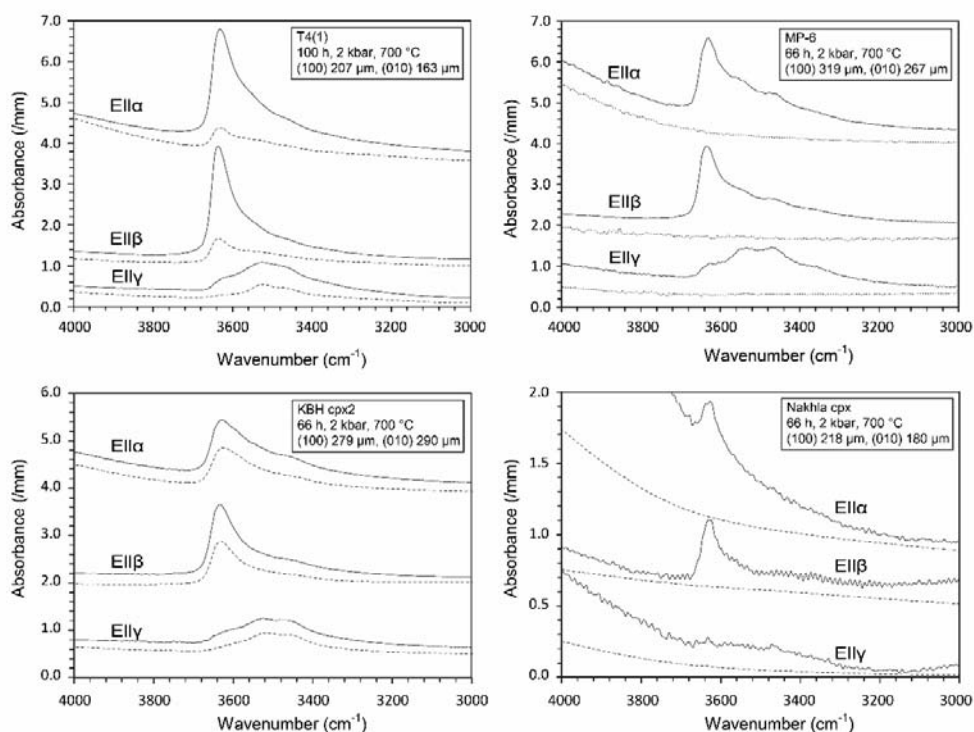
927   Figure 1
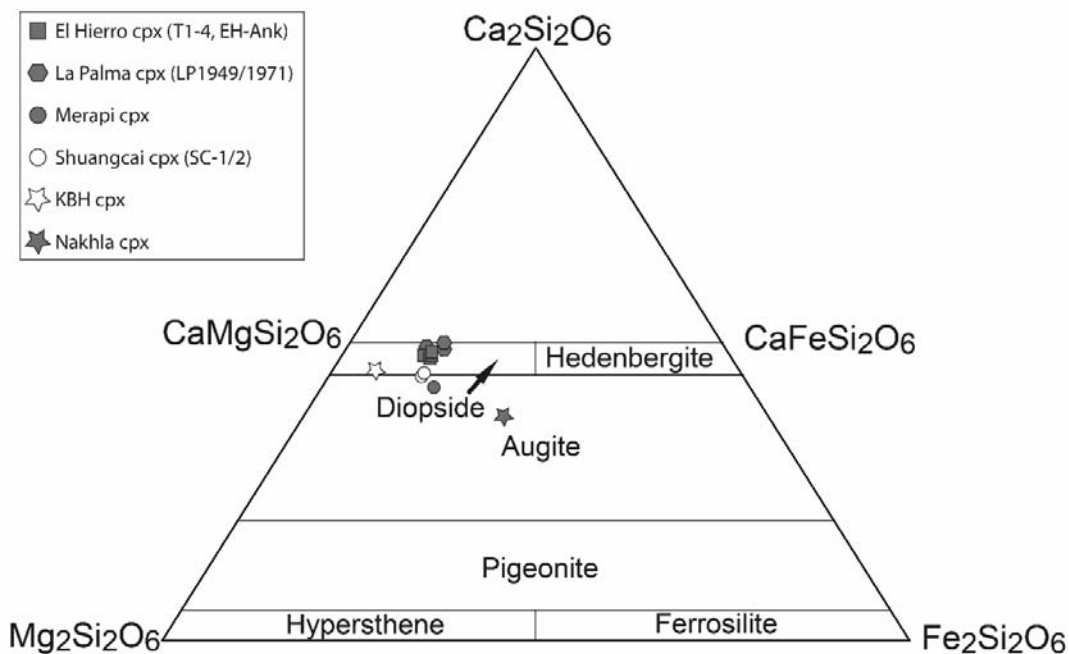
928

929   Figure 2

930

931

932
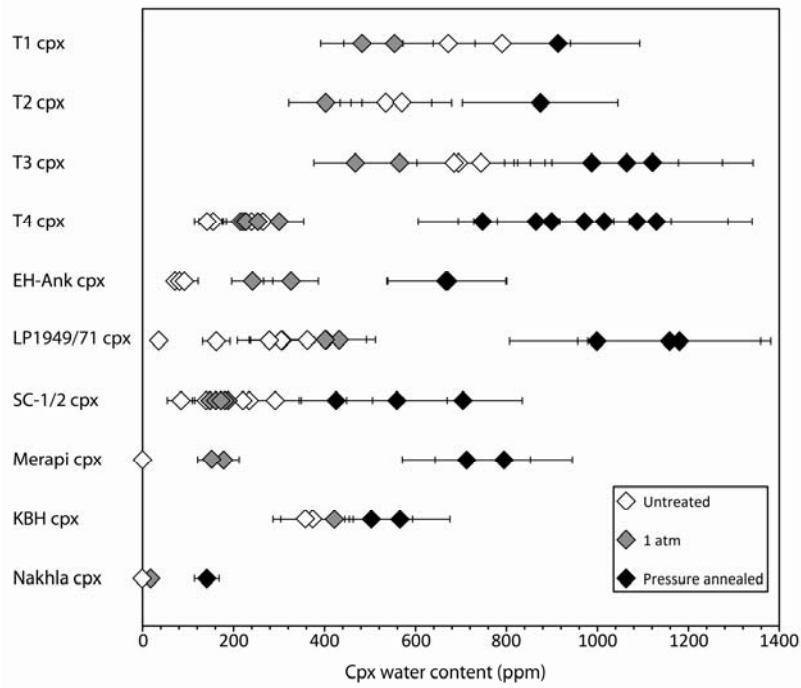
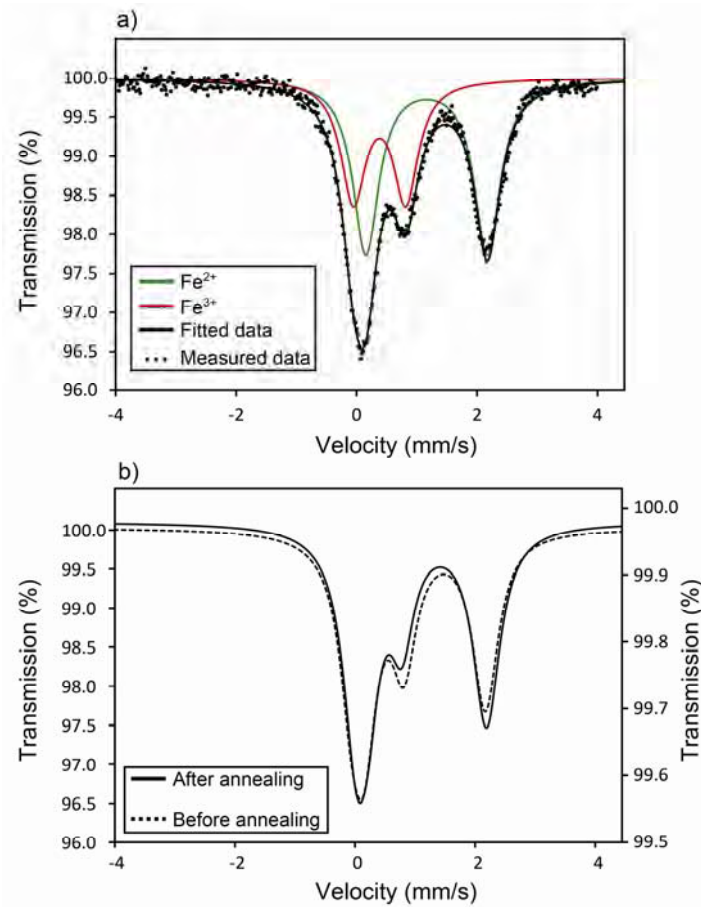40   Weis et al. American Mineralogist
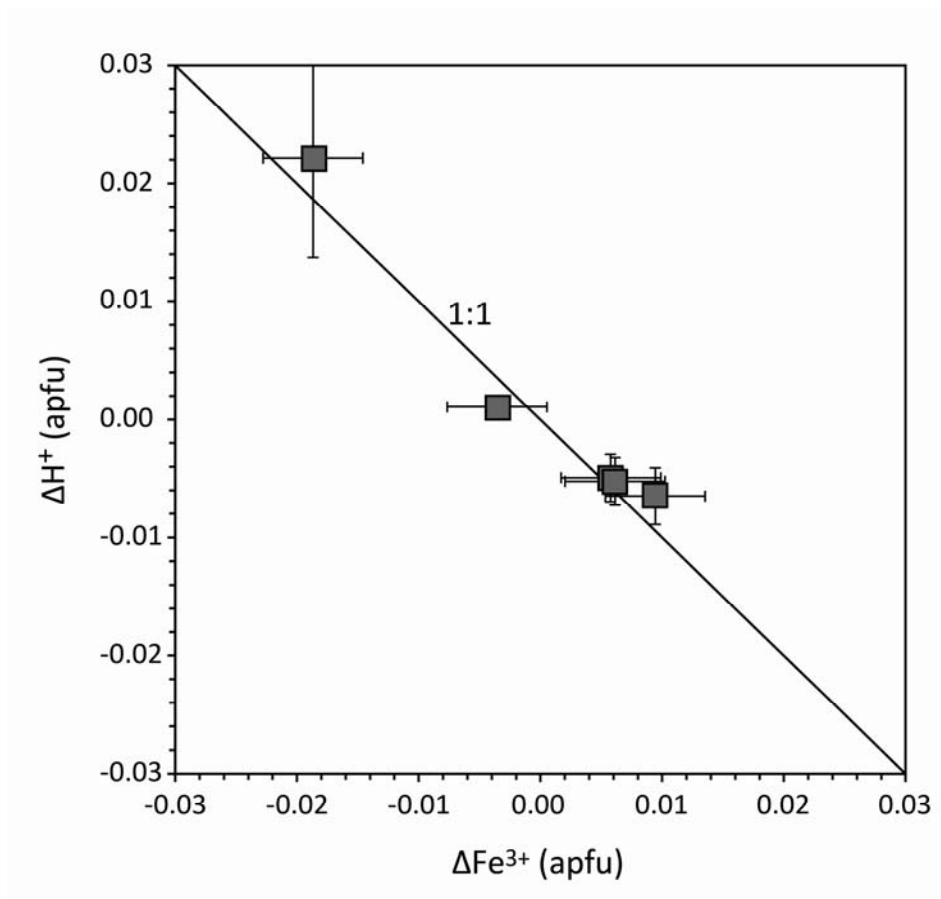
933   Figure 3

934

935   Figure 4

936

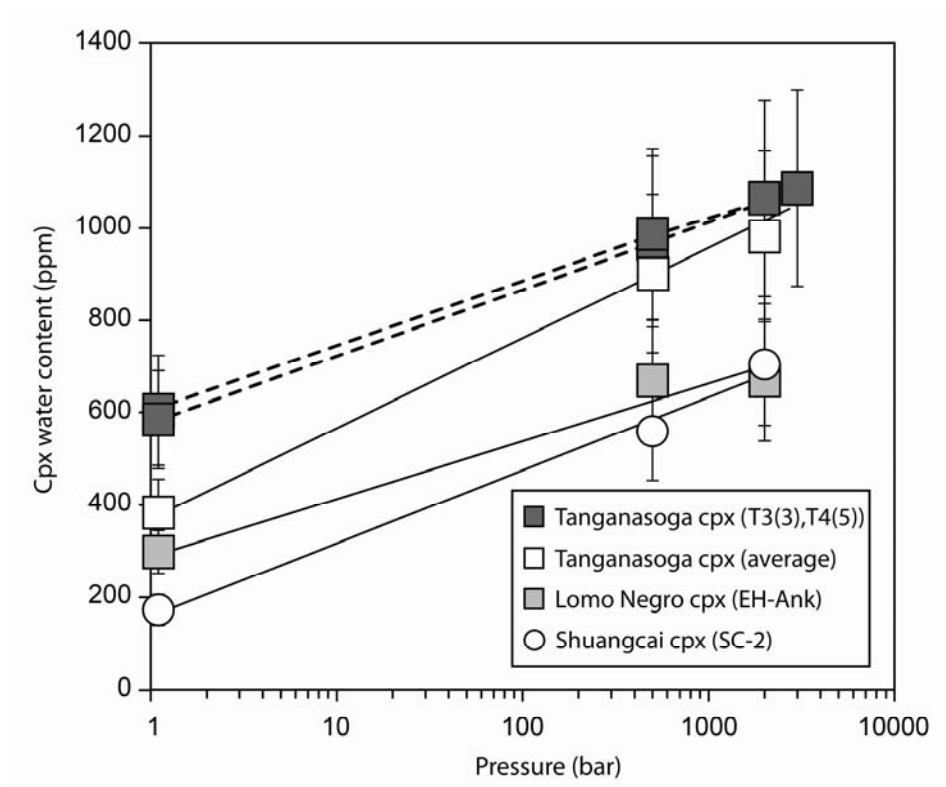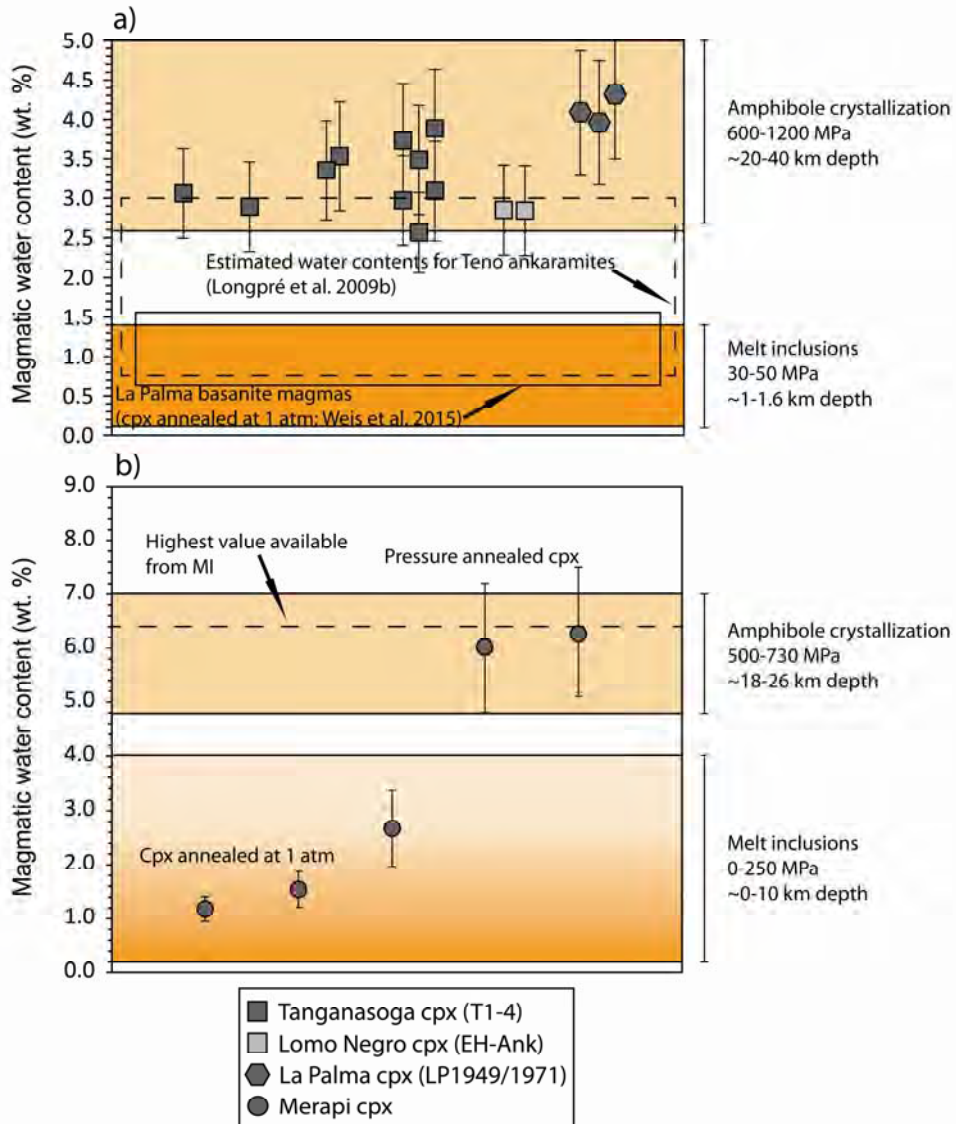937   Figure 5

938

939

940   Figure 6
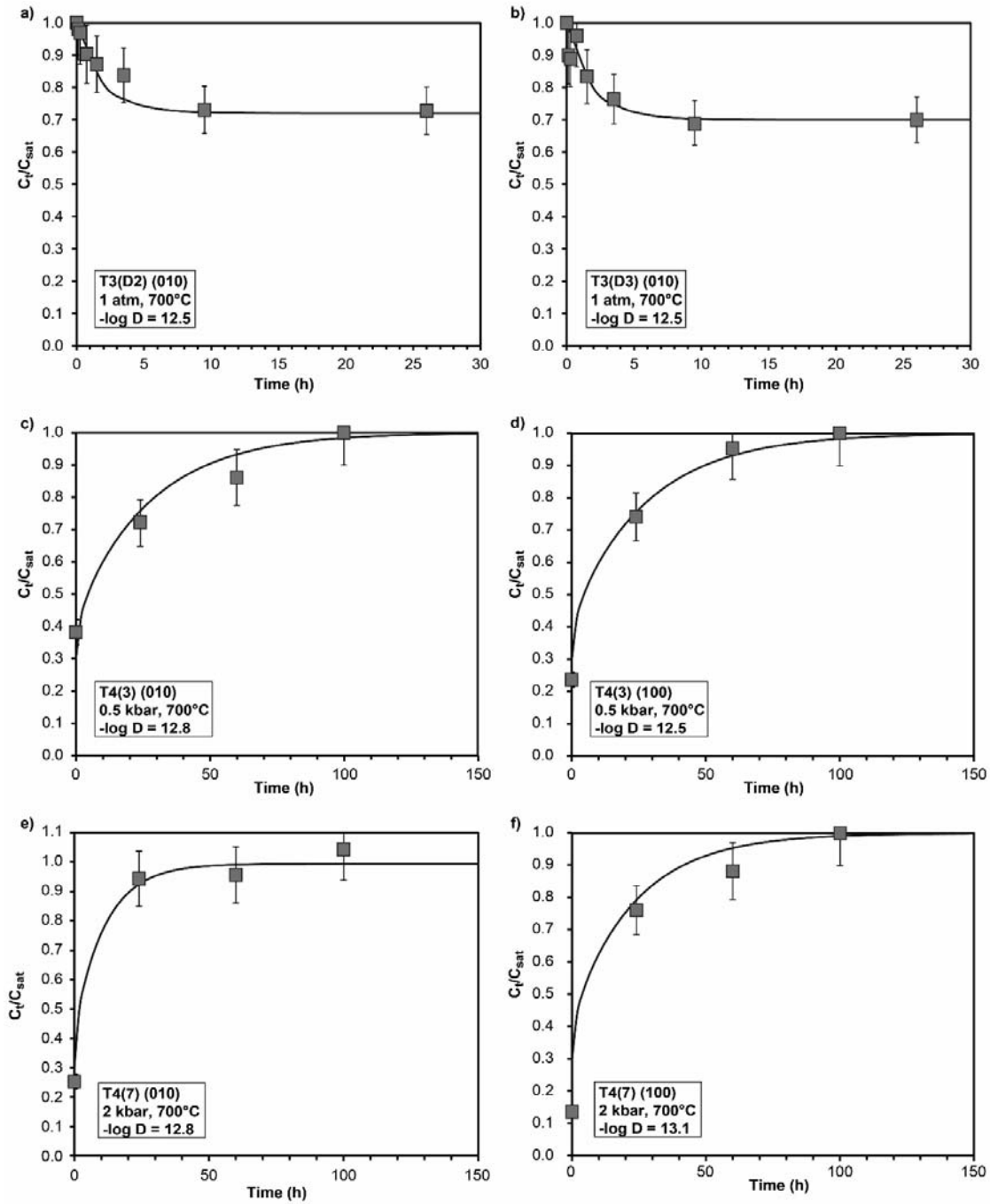
941

942   Figure 7

943

944   Figure 8

945

946 **Tables**

Table 1. Sample set used in this study.

Sample	Description	No. of cpx analyzed	Reference
Tanganasoga, El Hierro, Canary Islands			
T1	Ankaramite lava bomb	3	Carracedo et al 2001, Longpre et al. 2009a
T2	Ankaramite lava bomb	3	
T3	Ankaramite lava bomb	4	
T4	Ankaramite lava bomb	8	
Lomo Negro, El Hierro, Canary Islands			Villasante-Marcos & Pavón-Carrasco 2014
EH-Ank	Ankaramite lava flow	3	
Cumbre Vieja Rift, La Palma, Canary Islands			Brändle et al. 1974, Klügel et al. 2000
LP1971-B	Kaersutite cumulate xenolith, 1971 Teneguia eruption	4	
LP1971-1	Basanite lava, 1971 Teneguia eruption	1	
LP1949	Basanite lava, 1949 Hoyo Negro eruption	1	
Shuangcai volcano, Zejiang, China			Liu et al. (unpublished manuscript)
SC-1	Basanite lava, 5-10 Ma	4	
SC-2	Basanite lava, 5-10 Ma	4	
Merapi volcano, Java, Indonesia			Gertisser 2001, Ratdomopurbo et al. 2013
MP-BA06-KA2	Basaltic andesite lava, 2006 eruption	5	
Kilbourne Hole, New Mexico, USA			Kil & Wendlandt 2004, Harvey et al. 2012
KBH	Mantle xenolith	3	
Martian Meteorite			Bunch & Reid 1975, Treiman 1993
Nakhla	Ultramafic cumulate, Mars	1	

Table 2. Major elements and normalized cations of clinopyroxenes used in this study obtained by Electron Probe Micro Analysis (EPMA)[a]

Sample	SiO_2	Al_2O_3	MgO	Na_2O	MnO	TiO_2	K_2O	CaO	FeO	Cr_2O_3	Total
T1 average	47.486	6.247	13.441	0.510	0.095	3.015	0.004	22.659	6.702	0.060	100.217
T2 average	47.662	6.527	13.412	0.513	0.097	3.121	0.003	22.600	6.678	0.066	100.679
T3 average	47.439	6.675	13.466	0.492	0.098	3.160	0.002	22.635	6.606	0.046	100.618
T4 average	47.951	6.418	13.662	0.475	0.125	2.979	0.005	22.571	6.594	0.056	100.838
EH-Ank average[b]	48.145	5.582	13.409	0.566	0.092	2.434	0.006	22.377	6.721	0.067	99.398
LP1971-B average	47.020	6.330	12.200	0.644	0.148	2.583	0.009	22.771	7.186	0.079	98.970
LP1971-1 average[b]	47.132	6.672	12.364	0.663	0.156	2.479	0.006	22.488	7.550	0.081	99.591
LP1949 average[b]	47.989	5.976	13.211	0.561	0.097	2.417	0.005	22.806	6.320	0.119	99.501
SC-1(1)	49.912	3.022	15.482	0.409	0.149	1.042	0.003	21.388	6.818	0.210	98.434
SC-2(1)	50.682	3.420	17.225	0.489	0.145	0.725	0.000	18.513	6.963	0.359	98.521
SC-2(2)	49.335	3.717	14.877	0.443	0.112	1.297	0.006	21.830	6.817	0.200	98.636
MP-3	51.202	2.378	14.976	0.347	0.610	0.471	0.002	20.936	8.490	0.012	99.425
MP-6	50.455	2.412	14.747	0.346	0.527	0.468	0.005	21.150	8.350	0.017	98.476
MP-7	51.238	2.398	15.078	0.328	0.495	0.443	0.007	21.024	8.308	0.017	99.337
MP-8	47.226	5.811	13.716	0.549	0.115	2.506	0.005	22.729	6.461	0.044	99.161
KBH cpx	51.310	6.632	15.508	1.544	0.071	0.476	0.007	20.066	2.628	0.936	99.178
Nakhla cpx	51.272	0.914	12.763	0.230	0.453	0.238	0.003	18.993	14.045	0.348	99.259

Normalized cations:

Sample	Si^{4+}	Al^{3+}	Mg^{2+}	Na^+	Mn^{2+}	Ti^{4+}	K^+	Ca^{2+}	Fe^{2+}	Fe^{3+}	Cr^{3+}	Total
T1 average	1.756	0.272	0.741	0.037	0.003	0.084	0.000	0.898	0.149	0.058	0.002	4.000
T2 average	1.755	0.283	0.736	0.037	0.003	0.086	0.000	0.892	0.138	0.068	0.002	4.000
T3 average	1.747	0.290	0.739	0.035	0.003	0.087	0.000	0.893	0.145	0.058	0.001	4.000
T4 average	1.761	0.278	0.748	0.034	0.004	0.082	0.000	0.888	0.134	0.069	0.002	4.000
EH-Ank average	1.794	0.245	0.745	0.041	0.003	0.068	0.000	0.893	0.129	0.079	0.002	4.000
LP1971-B average	1.767	0.280	0.683	0.047	0.005	0.073	0.000	0.917	0.138	0.088	0.002	4.000
LP1971-1 average	1.759	0.293	0.688	0.048	0.005	0.070	0.000	0.899	0.138	0.098	0.002	4.000
LP1949 average	1.785	0.262	0.733	0.040	0.003	0.068	0.000	0.909	0.099	0.097	0.004	4.000
SC-1(1)	1.865	0.133	0.862	0.030	0.005	0.029	0.000	0.856	0.173	0.040	0.006	4.000
SC-2(1)	1.878	0.149	0.951	0.035	0.004	0.020	0.000	0.735	0.174	0.041	0.010	4.000
SC-2(2)	1.843	0.164	0.828	0.032	0.003	0.036	0.000	0.874	0.172	0.041	0.006	4.000
MP-3	1.907	0.104	0.831	0.025	0.019	0.013	0.000	0.835	0.210	0.054	0.000	4.000
MP-6	1.896	0.107	0.826	0.025	0.017	0.013	0.000	0.852	0.209	0.054	0.001	4.000
MP-7	1.908	0.105	0.837	0.023	0.016	0.012	0.000	0.839	0.206	0.053	0.001	4.000
MP-8	1.759	0.255	0.762	0.040	0.004	0.070	0.000	0.907	0.160	0.041	0.001	4.000
KBH cpx	1.864	0.284	0.840	0.109	0.002	0.013	0.000	0.781	0.068	0.012	0.027	4.000
Nakhla cpx[c]	1.958	0.041	0.726	0.017	0.015	0.007	0.000	0.777	0.440	0.009	0.011	4.000

[a]Major elements are given in wt.% oxide; [b]Values taken from Weis et al. 2015; [c]Dyar 2003 (Mössbauer data).

Table 3. Results for annealing of clinopyroxene at 1 atm.

Sample	Pressure	Starting value	15min	30min	45min	90min	180min	4h	8h	12h	16h	26h	34h	44h	60h	110h	278h
			Water content (ppm weight H_2O)														
T1(1)	1 atm	672												528	553		
T1(5)	1 atm	790						568	557	540		538		483	482		
T1(mös)	1 atm	706										493					
T2(3)	1 atm	569						411	474	416		420		395	402		
T2(mös)	1 atm	701										500					
T3(1)	1 atm	686						536	526	533		502		483	467		
T3(3)	1 atm	987										604					
T3(4)	1 atm	744	717	662	642	575	565										
T3(mös)	1 atm	659										394					
T4(2)	1 atm	154						173	202	214		246		253	253		
T4(5)	1 atm	228														288	299
T4(5)	1 atm	971										584					
T4(6)	1 atm	141									232		226				
T4(mös)	1 atm	263										307					
EH-Ank(1)	1 atm	91										241					
EH-Ank(3)	1 atm	81											290		326		
EH-Ank(3)	1 atm	670									354			298			
LP1971-B (1)	1 atm	314											434				
LP1971-B (2)	1 atm	309										409					
LP1971-B (3)	1 atm	279										406					
SC-1(2)	1 atm	84												149	164		
SC-1(3)	1 atm	239												181	182		
SC-1(4)	1 atm	137												158	142		
SC-2(3)	1 atm	292													173		
SC-2(4)	1 atm	221													183		
KBH cpx2	1 atm	565										456		454			
KBH cpx3	1 atm	379										379					
MP-4	1 atm	0										146		151			
MP-5	1 atm	0										177		177			
Nakhla	1 atm	0											16				

For blank space no measurement has been done.
Estimated uncertainty for water contents is ± 20 %.

947

Table 4. Results for pressure annealing of clinopyroxene.

Sample	Pressure	Starting value	24h	46h	60h	66h	72h	100h	120h	169h
						Water content (ppm weight H_2O)				
T1(1)	2 kbar	553							912	
T2(2)	2 kbar	535							874	
T3(3)	2 kbar	694							1064	
T3(3)	0.5 kbar	1064		987						
T4(1)	2 kbar	264	696		829			899		
T4(3)	0.5 kbar		545		674			747		
T4(4)	2 kbar	215								1015
T4(5)	3 kbar	315	797		927			1003		1086
T4(5)	0.5 kbar	1086					971			
T4(7)	2 kbar	221	949		1019			1129		
EH-Ank(2)	0.5 kbar	71					668			
EH-Ank(3)	2 kbar	326	670							
LP1971-B (5)	2 kbar	364				1180				
LP1971-1 (4)	2 kbar	162				1158				
LP1949 (5)	2 kbar	36				998				
SC-1(1)	2 kbar	110					425			
SC-2 (1)	2 kbar	193					704			
SC-2 (2)	0.5 kbar	202					559			
MP-6	2 kbar	0					794			
MP-7	2 kbar	0					712			
MP-8	0.5 kbar	0					768			
KBH cpx	2 kbar	357					503			
KBH cpx2	2 kbar	374					565			
Nakhla cpx	2 kbar	16					134			

For blank space no measurement has been done.
Estimated uncertainty for water contents is ± 20 %.

948

49

Weis et al. American Mineralogist

Table 5. Mössbauer spectroscopy results

Sample	int[a] (%)	fwhm (mm/s)	cs (mm/s)	dq (mm/s)
T1				
Fe^{2+}	72.0	0.58	1.10	2.16
Fe^{3+}	28.0	0.47	0.53	0.59
T2				
Fe^{2+}	66.8	0.54	1.08	2.17
Fe^{3+}	33.2	0.47	0.54	0.59
T3				
Fe^{2+}	71.5	0.54	1.10	2.15
Fe^{3+}	28.5	0.44	0.54	0.58
T4				
Fe^{2+}	66.1	0.55	1.09	2.15
Fe^{3+}	33.9	0.49	0.53	0.59
LP1971-B				
Fe^{2+}	61.2	0.39	1.07	2.20
Fe^{3+}	38.8	0.34	0.50	0.61
SC-1				
Fe^{2+}	81.1	0.53	1.12	2.09
Fe^{3+}	18.9	0.44	0.50	0.61
SC-2				
Fe^{2+}	80.8	0.58	1.12	2.13
Fe^{3+}	19.2	0.43	0.51	0.62
MP-BA06-KA2				
Fe^{2+}	79.6	0.50	1.10	2.08
Fe^{3+}	20.4	0.36	0.53	0.58
KBH cpx				
Fe^{2+}	85.5	0.56	1.15	2.12
Fe^{3+}	14.5	0.54	0.43	0.65

int - intensity in percentage of total absorption area [a]= Fe^{m+}/Fe_{total}
fwhm - full width at half maximum (including source width)
cs - centroid shift
dq - quadrupole splitting
Estimated uncertainty for intensities is ± 1 %.

949

Table 6. Mössbauer spectroscopy results for hydration experiments

Sample	int[a] (%)	fwhm (mm/s)	cs (mm/s)	dq (mm/s)	$[H_2O]_{cpx}$ (ppm)	$\Delta[Fe^{n+}]$ (%)	$\Delta[H_2O]_{cpx}$ (ppm)	$\Delta[H_2O]_{cpx}$ in (%) of Fe_{total}	$\Delta[H^+]_{cpx}$ (apfu)	$\Delta[Fe^{3+}]$ (apfu)	Ratio[b]
T1 mös											
Fe^{2+}	67.5	0.61	1.17	2.02	706	-2.9 ±2	-213	-2.5 ±1.0	-0.005	0.006	0.9
Fe^{3+}	32.5	0.59	0.37	0.91		2.9 ±2		2.5 ±1.0			
T1 mös H_2											
Fe2+	64.5	0.61	1.08	2.18	493						
Fe3+	35.5	0.54	0.52	0.59							
T2 mös											
Fe^{2+}	65.9	0.65	1.09	2.13	701	-2.8 ±2	-201	-2.4 ±1.0	-0.005	0.006	0.9
Fe^{3+}	34.1	0.63	0.51	0.60		2.8 ±2		2.4 ±1.0			
T2 mös H_2											
Fe^{2+}	63.1	0.61	1.08	2.17	500						
Fe^{3+}	36.9	0.56	0.51	0.60							
T3 mös											
Fe^{2+}	67.7	0.57	1.16	2.02	659	-4.6 ±2	-265	-3.2 ±1.2	-0.007	0.009	0.7
Fe^{3+}	32.3	0.60	0.37	0.88		4.6 ±2		3.2 ±1.2			
T3 mös H_2											
Fe^{2+}	63.1	0.57	1.17	2.01	394						
Fe^{3+}	36.9	0.59	0.38	0.87							
T4 mös											
Fe^{2+}	61.7	0.60	1.08	2.19	263	1.7 ±2	44	0.5 ±0.2	0.001	-0.003	0.3
Fe^{3+}	38.3	0.57	0.51	0.62		-1.7 ±2		-0.5 ±0.2			
T4 mös H_2											
Fe^{2+}	63.4	0.60	1.08	2.19	307						
Fe^{3+}	36.6	0.60	1.08	0.62							
T4(7)											
Fe^{2+}	60.2	0.52	1.16	2.02	221	9.2 ±2	908	10.9 ±4.4	0.022	-0.019	1.2
Fe^{3+}	39.8	0.50	0.38	0.87		-9.2 ±2		-10.9 ±4.4			
T4(7) Pressure											
Fe^{2+}	69.0	0.54	1.11	2.17	1129						
Fe^{3+}	31.0	0.48	0.50	0.57							

int - intensity in percentage of total absorption area [a]= Fe^{m+}/Fe_{total}
fwhm - full width at half maximum (including source width)
cs - centroid shift
dq - quadrupole splitting
Estimated uncertainty for intensities is ± 1 %.
$\Delta[Fe^{n+}]$ refers to the change in Fe^{m+}/Fe_{total} after annealing experiments
$\Delta[H_2O]_{cpx}$ refers to the measured water loss or gain in crystals after annealing experiments
$\Delta[H^+]_{cpx}$ refers to the loss or gain of hydrogen atoms in the investigated crystal
$\Delta[Fe^{3+}]$ refers to the change in Fe^{3+}/Fe_{total} after annealing experiments expressed in atoms per formula unit
[b]The ratio is given by $\Delta[H^+]_{cpx}/\Delta[Fe^{3+}]$

950

951

Table 7. Clinopyroxene dehydration

Time (hours)	T3 D2		T3 D3	
	$[H_2O]_{cpx}$ (ppm)[a]	C_t/C_0[b]	$[H_2O]_{cpx}$ (ppm)[a]	C_t/C_0[b]
0	382	1.00	469	1.00
0.13	376	0.98	422	0.90
0.25	370	0.97	418	0.89
0.75	345	0.90	450	0.96
1.5	333	0.87	391	0.83
3.5	320	0.84	358	0.76
9.5	279	0.73	324	0.69
26	278	0.73	328	0.70

[a]Concentration representative of (010), i.e. $A_\alpha + A_\gamma$
[b]C_0 = starting value C_t = concentration after time t

952

Table 8. Calculated primary magmatic water contetns

Sample	[H$_2$O]$_{cpx}$ after annealing (ppm)	$^{(IV)}$Al$^{3+\,a}$	Ca$^{2+\,a}$	lnD$_{(cpx-melt)}$	D$_{(cpx-melt)}$	[H$_2$O]$_{Melt}$ (wt. %)
T1	912	0.244	0.898	-3.513	0.030	3.06 ±0.62
T2(2)	874	0.245	0.892	-3.499	0.030	2.89 ±0.58
T3(3)	1064	0.253	0.893	-3.450	0.032	3.35 ±0.68
T3(4)	1121	0.253	0.893	-3.450	0.032	3.53 ±0.70
T4	899	0.239	0.888	-3.537	0.029	3.09 ±0.62
T4(2)	865	0.239	0.888	-3.537	0.029	2.97 ±0.60
T4(3)	747	0.239	0.888	-3.537	0.029	2.57 ±0.52
T4(4)	1015	0.239	0.888	-3.537	0.029	3.49 ±0.70
T4(5)	1086	0.239	0.888	-3.537	0.029	3.73 ±0.74
T4(7)	1129	0.239	0.888	-3.537	0.029	3.88 ±0.78
EH-Ank(2)	668	0.206	0.893	-3.751	0.023	2.84 ±0.56
EH-Ank(3)	670	0.206	0.893	-3.751	0.023	2.85 ±0.58
LP1971-B (5)	1180	0.233	0.917	-3.600	0.027	4.32 ±0.86
LP1971-1(4)	1158	0.241	0.899	-3.532	0.029	3.96 ±0.80
LP1949 (5)	998	0.215	0.909	-3.712	0.024	4.08 ±0.82
MP-4[b]	151	0.096	0.842	-4.416	0.012	1.25 ±0.24
MP-5[b]	177	0.096	0.842	-4.416	0.012	1.46 ±0.30
MP-6	794	0.103	0.851	-4.379	0.013	6.34 ±1.26
MP-7	712	0.092	0.838	-4.440	0.012	6.03 ±1.20
MP-8	768	0.241	0.907	-3.544	0.029	2.66 ±0.54

Calculated uncertainties (2 s.d.) for $^{(IV)}$Al^{3+} and Ca^{2+}are ± 0.010 and ± 0.007 for D$_{(cpx-melt)}$
Estimated uncertainties for water contents are ± 20 % for CPX and magmas
[a]average values from Table 2
[b]values for $^{(IV)}$Al^{3+} and Ca^{2+}are based on averages from crystals MP-3, MP-6 and MP-7

953

53   Weis et al. American Mineralogist